Journal of Geophysical Research: Oceans

RESEARCH ARTICLE
10.1029/2018JC014533

Examining the Impact of Tropical Cyclones on Air-Sea CO_2 Exchanges in the Bay of Bengal Based on Satellite Data and In Situ Observations

Haijun Ye[1], Jinyu Sheng[1,2], Danling Tang[1], Evgeny Morozov[1], Muhsan Ali Kalhoro[1,3], Sufen Wang[1], and Huabing Xu[1]

[1]State Key Laboratory of Tropical Oceanography, Guangdong Key Lab of Ocean Remote Sensing, South China Sea Institute of Oceanology, Chinese Academy of Sciences, Guangzhou, China, [2]Department of Oceanography, Dalhousie University, Halifax, Nova Scotia, Canada, [3]Faculty of Marine Sciences, Lasbela University of Agriculture, Water and Marine Sciences, Uthal, Pakistan

Key Points:
- TCs tended to increase the pCO_{2sea} in the postmonsoon and to decrease the pCO_{2sea} in the premonsoon in the Bay of Bengal
- Large vertical differences in the ratio of DIC to TA in the upper layer were responsible for increasing pCO_{2sea} induced by TCs
- TCs were estimated to account for 55 ± 23% of the annual-mean CO_2 annual efflux

Correspondence to:
D. Tang,
lingzistdl@126.com

Citation:
Ye, H., Sheng, J., Tang, D., Morozov, E., Kalhoro, M. A., Wang, S., & Xu, H. (2019). Examining the impact of tropical cyclones on air-sea CO_2 exchanges in the Bay of Bengal based on satellite data and in situ observations. *Journal of Geophysical Research: Oceans*, *124*, 555–576. https://doi.org/10.1029/2018JC014533

Received 6 SEP 2018
Accepted 16 NOV 2018
Accepted article online 28 NOV 2018
Published online 25 JAN 2019

Abstract The impact of tropical cyclones (TCs) on the CO_2 partial pressure at the sea surface (pCO_{2sea}) and air-sea CO_2 flux (F_{CO2}) in the Bay of Bengal (BoB) was quantified based on satellite data and in situ observations between November 2013 and January 2017. The in situ observations were made at the BoB Ocean Acidification mooring buoy. A weak time-mean net source of 55.78 ± 11.16 mmol CO_2 m^{-2} $year^{-1}$ at the BoB Ocean Acidification site was estimated during this period. A wide range in increases of pCO_{2sea} (1.0–14.8 μatm) induced by TCs occurred in postmonsoon (October–December), and large decreases of pCO_{2sea} (−14.0 μatm) occurred in premonsoon (March–May). Large vertical differences in the ratio of dissolved inorganic carbon (DIC) to total alkalinity (TA) in the upper layer (ΔDIC/TA) were responsible for increasing pCO_{2sea} in postmonsoon. Relatively small values of ΔDIC/TA were responsible for decreasing pCO_{2sea} in premonsoon. Five TCs (Hudhud, Five, Kyant, Vardah, and Roanu) were considered. Hudhud significantly enhanced CO_2 efflux (18.49 ± 3.70 mmol CO_2/m^2) in oversaturated areas due to the wind effect during the storm and *wind-pump* effects after the storm. Vardah insignificantly changed F_{CO2} (1.22 ± 0.24 mmol CO_2/m^2) in undersaturated areas because of the counteraction of these two effects. Roanu significantly enhanced CO_2 efflux (19.08 ± 3.82 mmol CO_2/m^2) in highly oversaturated conditions ($\Delta pCO_2 > 20$ μatm) since the wind effect greatly exceeded the wind-pump effects. These five TCs were estimated to account for 55 ± 23% of the annual-mean CO_2 annual efflux, suggesting that TCs have significant impacts on the carbon cycle in the BoB.

Plain Language Summary We examined the impact by five tropical cyclones on the sea surface pCO_2 and air-sea CO_2 exchange using Bay of Bengal Ocean Acidification moored buoy measurements over the Bay of Bengal. To our knowledge, this is the first study on the different effects of tropical cyclones and vertical differences in the ratio of dissolved inorganic carbon to total alkalinity in the upper layer on the sea surface pCO_2 and local air-sea CO_2 flux.

1. Introduction

With a steady increase in the atmospheric CO_2 concentration, the ocean plays a more important role than ever in mitigating climate changes (Le Quéré et al., 2009, 2016). The oceanic storage of the anthropogenic CO_2 is affected significantly by the air-sea CO_2 flux (F_{CO2}) at the sea surface (Takahashi et al., 2009). The latter depends on the difference between the partial pressure of CO_2 at the sea surface (pCO_{2sea}) and in the overlying atmosphere (pCO_{2air}), the wind speed, sea surface temperature (SST), and sea surface salinity (SSS, Wanninkhof, 1992, 2014; Wanninkhof et al., 2009). Among these factors, the wind speed plays a very important role in determining the absolute value of F_{CO2} due to the quadratic or cubic functional dependence of the gas transfer velocity with the wind speed. The gas transfer velocity is one of the key parameters for estimating F_{CO2} (Wanninkhof, 1992, 2014; Wanninkhof et al., 2009; Wanninkhof & McGillis, 1999).

The study region of this paper is the Bay of Bengal (BoB), which is a large but relatively shallow embayment of the northeastern Indian Ocean, with a total surface area of about 2.17×10^6 km^2 (Figure 1a). The BoB is highly influenced by the southwest monsoon in summer (June–September) and the northeast monsoon in winter (November–February, Thadathil et al., 2007). The Bay also experiences intense tropical cyclones (TCs) during both the premonsoon months (March–May) and postmonsoon months (October–December,

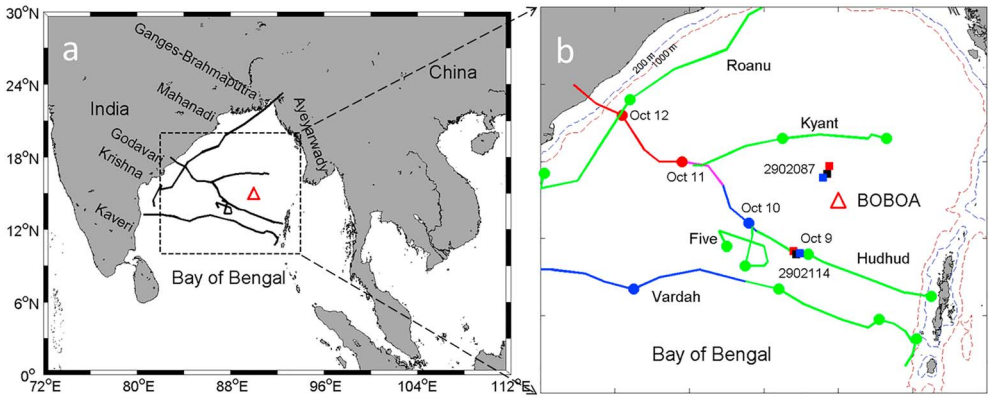

Figure 1. (a) Map showing the Bay of Bengal (BoB), tracks of five tropical cyclones (TCs), and the location of the Research Moored Array for African-Asian-Australian Monsoon Analysis and Prediction (RAMA) mooring at 90°E and 15°N (red triangle). (b) The tracks and intensity of five TCs including Hudhud (8–12 October 2014), Five (6–7 November 2014), Kyant (25–26 October 2016, C3), Vardah (7–11 December 2016, C4), and Roanu (18–21 May 2016). The storm intensity is marked by color lines (green: tropical storm; blue: TC 1; pink: TC 2; red: TC 3, and dark red: TC 4). Solid red, black, and blue squares represent Argo float stations before, during, and after the TC's passage. Blue and brown dashed lines represent 200- and 1,000-m water depths. Red triangle represents the BOBOA mooring site. BOBOA = BoB Ocean Acidification.

Neetu et al., 2012; Obasi, 1997). The BoB receives a large volume of freshwater from precipitations and from rivers including the Ayeyarwady, Ganges-Brahmaputra, Mahanadi, Godavari, Krishna, and Kaveri Rivers (Sengupta et al., 2006). The total freshwater input to the BoB north of 14°N during the summer monsoon is about 3,050 km^3, including 1,250 km^3 from precipitation and 1,800 km^3 of runoff from rivers (Sengupta et al., 2006). This leads to the low surface salinity ($<$ 30 psu), low total alkalinity (TA, $<$ 2,200 μmol/kg), and low dissolved inorganic carbon (DIC, $<$ 1,900 μmol/kg) in the BoB in the postmonsoon (Bates et al., 2006; Sabine et al., 2002). The ratio of the DIC to TA (henceforth DIC/TA) increases from about 0.85 at the sea surface to 0.96 at depths with the potential density of 26.0 kg/m^3 (Sabine et al., 2002). Large values of DIC/TA were found to influence the effect of temperature changes on pCO_2 (Goyet et al., 1993).

A very few pCO_2 observations were made previously in the BoB. As a result, the mean seasonal pCO_2 cycle was not very well known (Takahashi et al., 2009). A large pCO_2 seasonality (up to 100 μatm) in the BoB was suggested by Bates et al. (2006). A recent synthesis analysis indicated, however, a relatively low pCO_2 seasonality (about 25 μatm) but significant pCO_2 variations in April–May in the Bay (Sarma et al., 2013). Previous studies also provided very different estimations of F_{CO2} in the BoB. Based on the inorganic carbon data collected in the Indian Ocean in 1995, for example, Bates et al. (2006) suggested that the BoB is a net oceanic source of atmospheric CO_2. Takahashi et al. (2009) constructed the climatological mean distribution for the sea surface water pCO_2 over the global oceans based on the observations from 1970 and 2007, and they suggested that the BoB is near equilibrium for the CO_2. By examining numerical results produced by various ocean biogeochemical models and different atmospheric inversions, Sarma et al. (2013) argued that the BoB is a small annual net sink region for the atmospheric CO_2. These different estimations are due partially to the paucity of sampling or various methods used to estimate the fluxes, and partially to the effects of extreme weather events such as typhoons and TCs, which were not be taken into account in the previous estimates. In addition, the large seasonal variation of pCO_2 suggested by Bates et al. (2006) was confirmed by the recent Surface Ocean CO_2 Atlas database (Bakker et al., 2016).

Several previous studies suggested that TCs (or typhoons) are responsible for the cooling of sea surface temperature (SST) behind storms (Maneesha et al., 2012; Sengupta et al., 2008; Vidya & Das, 2017; Warner et al., 2016) and increase of chlorophyll a (Chl*a*) concentrations based on ocean-color satellite data and in situ observations (Chacko, 2017; Chen et al., 2013; Sarangi et al., 2015; Vidya & Das, 2017) in the BoB and other regions due to the storm-induced *wind-pump* effects (Sheng et al., 2006; Song & Tang, 2017; Ye et al., 2013). It was found that the storm-induced SST cooling is about 3 times larger during the premonsoon season than during the postmonsoon season because of the thick barrier layer (BL) and deep thermocline in winter (Neetu et al., 2012; Sengupta et al., 2008). By wind-pump effects, the storm-induced vertical mixing and

upwelling can decrease the SST, resulting in decreasing the pCO_{2sea} by 0.0423 °C^{-1} (Takahashi et al., 1993), and also increasing the DIC, which increases the pCO_{2sea} (Sun et al., 2014; Ye, Sheng, et al., 2017).

A TC is a very intense and localized atmospheric low-pressure system formed over tropical oceans typically with strong winds and high precipitations. Previous studies demonstrated that the passage of a TC can lead to enormous F_{CO2} from the surface ocean to the atmosphere, based on analyses of various moored buoy data (Bates et al., 1998; Bates, 2007; Bond et al., 2011; Nemoto et al., 2009), underway measurements (Perrie et al., 2004; Sun et al., 2014; Ye, Sheng, et al., 2017), and model results (Huang & Imberger, 2010; Wada et al., 2013). Some studies suggested that TCs have significant impacts on the local inorganic carbon system such as in the South China Sea, East China Sea, and Atlantic Ocean (Bates, 2007; Bates et al., 1998; Huang & Imberger, 2010; Nemoto et al., 2009; Ye, Sheng, et al., 2017). Other studies implied that TCs have weak contributions on the global carbon cycle (Levy et al., 2012). The current wisdom is that the actual impact of a TC on F_{CO2} depends on the oceanographic condition at the time of the TC passage. One of important scientific issues is whether the TCs have a significant impact on the pCO_{2sea} and F_{CO2} in the BoB. This study is to address this issue by examining the changes in pCO_{2sea} and F_{CO2} caused by five TCs in the premonsoon and postmonsoon using remote sensing data and in situ oceanographic observations made at the BoB Ocean Acidification (BOBOA) mooring buoy. Five TCs during the study period between November 2013 and January 2017 were considered. There were four other TCs passing though the BoB during the study period, including TC Madi on 6–12 December 2013, TC One on 4–5 January 2014, TC Two on 29–30 July 2015, and TC Nada on 29 November to 1 December 2016. Since these four TCs were far away from the BOBOA site, their effects were not considered here. The main purpose of this paper is to characterize the importance of vertical differences in DIC/TA controlling the pCO_{2sea} variation and to evaluate the influence of TCs on the local F_{CO2} in the BoB.

This paper is organized as follows. The data and methodology used in this study are presented in section 2. The in situ observations and satellite remote sensing data in the BoB during TC Hudhud are examined in section 3. The temporal variability of pCO_{2sea} and F_{CO2} induced by TC Hudhud and other four TCs, and estimation of the total F_{CO2} induced by TCs are discussed in section 3.5. Conclusions of this study are presented in section 4.

2. Data and Methods

2.1. RAMA Buoy Data

In November 2007, the Pacific Marine Environment Laboratory and Indian technicians deployed a Research Moored Array for the African-Asian-Australian Monsoon Analysis and Prediction (RAMA) in the BoB (McPhaden et al., 2009). Each buoy was equipped with a suite of meteorological, physical, and biogeochemical sensors. The BOBOA mooring buoy was deployed in November 2013 as part of the RAMA array. A Moored Autonomous pCO_2 ($MAPCO_2$) system was mounted on the buoy. For a detailed description of the $MAPCO_2$ system and associated data processing, a reader is referred to Sutton et al. (2014). In brief, the $MAPCO_2$ system utilized an automated equilibrator-based gas collection system to measure the mole fraction of CO_2 (xCO_2) in the surface seawater every 3 hr, in addition to sample temperature, pressure, and relative humidity. The xCO_2 measurement was made by a LI-820, LI-COR gas analyzer calibrated with reference gases traceable to World Meteorological Organization standards. A Sea-Bird Electronics 16 plus V2 SeaCAT was also deployed and integrated with the $MAPCO_2$ system to make SST and SSS measurements used to calculate pCO_2 (Dickson et al., 2007; Sutton et al., 2016; Weiss, 1974). The accuracy of measuring the SST and SSS was about ±0.02 °C and ±0.02 psu, respectively (McPhaden et al., 2009). The overall uncertainty of the $MAPCO_2$ was better than 2 μatm for pCO_{2sea} and better than 1 μatm for pCO_{2air} (Sutton et al., 2014). The pCO_2 data were acquired between 24 November 2013 and 10 June 2015, and between 6 March 2016 and 9 January 2017 (Sutton et al., 2016; Sutton, Sabine, et al., 2017).

The RAMA mooring buoy data including the 10-min interval observations of radiation, wind velocity, precipitation and SST, and hourly observations of sea level pressure (SLP), SSS, and heat flux data, together with the three-hourly observations of pCO_2, SST, and SSS from the BOBOA mooring buoy, were used in this study. The wind observations were not available between 16 August 2016 and 10 January 2017. As a result, the 6-hourly cross-calibrated multiplatform (CCMP) winds were averaged to daily winds for the cases of TCs Kyant and Vardah. More information on the in situ observational data can be found from the webpage for the

Table 1
Statistics of Water Properties and CO_2 Fluxes (±Uncertainty) During Passages of Five Tropical Cyclones in the Bay of Bengal During the 39-Month Period From November 2013 to January 2017

Date	Tropical cyclone	Wind speed (m/s)	Mean ΔpCO_2 (μatm)	$dpCO_{2sea}$ (μatm)	dF_{CO2} (mmol CO_2/m^2)	dSST (°C)	dSSS (psu)	MLD (m)	ILD (m)	ΔDIC/TA
8–11 Oct 2014	Hudhud	12.0 ± 1.6	8.1 ± 4.7	14.8 ± 9.7	18.49 ± 3.70	−0.8 ± 0.3	0.9 ± 0.1	20	60	0.047 ± 0.028[b]
4–7 Nov 2014	Five	7.2 ± 2.3	3.2 ± 5.1	1.0 ± 6.2	−0.22 ± 0.04	−0.5 ± 0.3	0.2 ± 0.3	20	60	0.048 ± 0.028[b]
22–25 Oct 2016	Kyant	8.5 ± 1.2[a]	−3.8 ± 1.7	4.0 ± 5.8	−3.86 ± 0.77	−0.3 ± 0.2	0.2 ± 0.1	40	80	0.042 ± 0.027[b]
7–10 Dec 2016	Vardah	10.6 ± 0.6[a]	−6.9 ± 2.9	1.5 ± 7.5	1.22 ± 0.24	−0.2 ± 0.2	0.0 ± 0.1	40	80	0.046 ± 0.027[b]
18–21 May 2016	Roanu	10.5 ± 1.5	28.0 ± 7.6	−14.0 ± 11.8	19.08 ± 3.82	−1.2 ± 0.4	0.8 ± 0.3	5	20	0.003 ± 0.014[c]

Note. Uncertainties (±) represent 1 standard deviation. The wind speed is averaged from the tropical cyclone date; the mean ΔpCO_2 is defined as the 4-day mean value before the tropical cyclone date; $dpCO_{2sea}$, the dSST, and dSSS are defined as the difference in pCO_{2sea}, SST, and SSS between the 4-day averaged value after and before the tropical cyclone date, respectively; the dF_{CO2} is defined as the difference in F_{CO2} between the 8-day value after and the 4-day value before the tropical cyclone date. The pCO_2 is obtained from the National Oceanographic and Atmospheric Administration's PMEL (www.pmel.noaa.gov/, Sutton et al., 2016; Sutton, Sabine, et al., 2017). ΔDIC/TA is defined as the difference in DIC/TA between L_1 and L_2, where L_1 is the upper depth of ILD, and L_2 is the depth within the layer between ILD and the depth at which water temperature is cooler by 3 °C than the SST. SST = sea surface temperature; ILD = the depth of the top of the thermocline; DIC/TA = dissolved inorganic carbon/total alkalinity; WOCE = World Ocean Circulation Experiment; PMEL = Pacific Marine Environment Laboratory; SSS = sea surface salinity; GO-SHIP = Global Ocean Ship-based Hydrographic Investigations Program.
[a]The wind speed is extracted from the cross-calibrated mutiplatform winds. [b]The concentrations of DIC and TA in L_2 were derived from the DIC-salinity and TA-salinity relationships in the depth within the layer between ILD and 500 m based on the WOCE cruise in October 1995 (DIC = 215.3 × salinity − 5322.5, R^2 = 0.46, $P < 0.001$, n = 100; TA = 82.9 × salinity − 587.9, R^2 = 0.76, $P < 0.001$, n = 100). [c]The concentrations of DIC and TA in L_2 were derived from the DIC-salinity and TA-salinity relationships in the depth within the layer between ILD and 500 m based on two GO-SHIP cruises in April 2007 and April 2016 (DIC = 103.57 × salinity^2 − 6849.6 × salinity + 115115, R^2 = 0.96, $P < 0.001$, n = 294; TA = 21.78 × salinity^2 − 1422.3 × salinity + 25414, R^2 = 0.94, $P < 0.001$, n = 295).

National Oceanographic and Atmospheric Administration's Pacific Marine Environment Laboratory (www.pmel.noaa.gov/).

Since the observed winds at buoys were available only at a limited number of buoy locations, and F_{CO2} is commonly calculated using satellite wind products, the observed wind speed was converted to the wind speed at a height of 10 m above the mean sea level (MSL) based on (Large & Pond, 1981; Sutton, Wanninkhof, et al., 2017):

$$u_{10} = \frac{u(z)}{1 + \frac{\sqrt{Cd10}}{0.4} \times \ln\left(\frac{z}{10}\right)} \quad (1)$$

where u_{10} is the wind speed at 10 m from the MSL in meter per second, z is the height (m) of the wind sensor (4 m), $u(z)$ is the wind speed recorded by the moored sensor in meter per second, $Cd10$ is the drag coefficient set to be 0.0011, and 0.4 is von Karman's constant. The accuracy of the wind speed observations was about ±0.3 m/s or 3% (McPhaden et al., 2009). To calculate the F_{CO2}, the 10-min observed winds were averaged to 3-hourly winds.

2.2. TC and Satellite Data

Five TCs (Hudhud, Five, Kyant, Vardah, and Roanu) during the 39-month period between November 2013 and January 2017 were considered in this study (Table 1). The 6-hourly track data of each TC, including the central locations and maximum sustained wind speeds at 10 m above the MSL, were obtained from the Joint Typhoon Warning Center (weather.unisys.com/hurricane/). Among these five TCs, Hudhud, Five, Kyant, and Vardah swept the BoB during the postmonsoon seasons and Roanu swept the region during the premonsoon seasons. It should be noted that the BOBOA mooring buoy was about 183–309 km away from storm centers of TCs Hudhud, Five, Kyant, and Vardah, and about 538 km away from TC Roanu (Figure 1b). Therefore, the in situ observations at the BOBOA mooring site may not represent the maximum changes in the oceanographic conditions over areas influenced directly by these five storms.

The 6-hourly CCMP winds with a horizontal resolution of 0.25° × 0.25° were obtained from the website for the Remote Sensing Systems at ftp://data.remss.com/measurements/ccmp/ (Atlas et al., 2011). The daily satellite remote sensing fields of 10-m winds and wind stress vector ($\vec{\tau}$) with a 0.25° × 0.25° resolution were obtained from the Advanced Scatterometer website at ftp.ifremer.fr/ifremer/cersat/products/gridded/MWF/L3/ASCAT/. The daily microwave and infrared (MW_IR) optimally interpolated SST products with a spatial resolution of 9 km were obtained from the website for the Remote Sensing Systems at ftp://data.remss.com/. The daily Moderate Resolution Imaging Spectroradiometer Aqua-derived sea surface phytoplankton Chl*a* product with a horizontal resolution of 4 km was obtained from the website of the NASA Ocean Color at oceancolor.gsfc.nasa.gov/. Daily fields of geostrophic velocities at the sea surface derived from the merged altimeter products and merged sea level anomaly (SLA) were extracted from the Archiving Validation and Interpretation of Satellite Oceanographic data at www.aviso.oceanobs.com.

2.3. ΔDIC/TA and Ekman Pumping Velocity

The surface mixed layer depth (MLD) and the Ekman pumping velocity (EPV) are used in this study to estimate the storm-induced vertical mixing and upwelling (or downwelling) during the passage of the TC. The MLD is defined as the depth at which the potential density is 0.125 kg/m^3 higher than the surface potential density (Girishkumar et al., 2014; Levitus, 1982). The ILD, the depth of the top of the thermocline, is defined as the depth at which the water temperature is cooler by 1 °C than

the SST (Rao & Sivakumar, 2003). The BL is defined as the layer between the bottom of the surface mixed layer and the top of the thermocline (Thadathil et al., 2007).

The EPV was calculated from the surface wind stress vector ($\vec{\tau}$) as follows:

$$\mathrm{EPV} = -\mathrm{Curl}_z\left(\frac{\vec{\tau}}{\rho_o f}\right) \tag{2}$$

where ρ_0 is the sea water density set to 1,025.0 kg/m^3 and f is the Coriolis parameter.

In this study, ΔDIC/TA is defined as the difference in DIC/TA between L_1 and L_2, where L_1 is the upper depth of ILD, and L_2 is the depth within the layer between ILD and the depth at which water temperature is cooler by 3 °C than the SST.

2.4. Estimation of Air-Sea CO_2 Flux

The flux of CO_2 across the air-sea interface (hereafter F_{CO2}) is often estimated from the bulk formula given as

$$F_{CO2} = k \times K_H \times \Delta \mathrm{pCO_2} \tag{3}$$

where k is the gas transfer velocity of CO_2, K_H is the solubility of CO_2 in seawater that is a function of salinity and temperature (Weiss, 1974), and ΔpCO_2 is the difference between pCO_{2sea} and pCO_{2air} defined as

$$\Delta pCO_2 = \mathrm{pCO_{2sea}} - \mathrm{pCO_{2air}} \tag{4}$$

A positive value of F_{CO2} represents the net CO_2 flux from sea to atmosphere (efflux), and a negative value represents the net CO_2 exchange from atmosphere to sea (influx). The transfer velocity, k, depends on u_{10} and the Schmidt number (S_c). The updated relationship established by Wanninkhof (2014) was used in this study to calculate k:

$$k = 0.251 {u_{10}}^2 (S_c/660)^{-0.5} \tag{5}$$

where S_c is a function of temperature (Wanninkhof, 2014).

Here we estimate approximately the uncertainty of F_{CO2} ($\delta_{F_{CO2}}$) from errors for three variables k, K_H, and ΔpCO_2 (defined, respectively, as δ_k, δ_{K_H}, and $\delta_{\Delta pCO_2}$ based on equation (3)). The uncertainty of K_H is about 0.3% (Weiss, 1974), and of ΔpCO_2 is 3 μatm or 0.8%. The cumulative error of k in equation (5) is about 19% (20%), which includes the uncertainty of 10% in the coefficient *0.251*, 3% in in situ wind speeds (4% in CCMP winds), 5% in S_c, and ad hoc additive uncertainty in k when wind speeds less than 3.5 m/s and greater than 12 m/s (Wanninkhof, 2014). Assuming that the errors for three variables are independent, the uncertainty for F_{CO2} can be estimated from

$$\delta_{F_{CO2}} = \sqrt{\delta_k^2 + \delta_{K_H}^2 + \delta_{\Delta pCO_2}^2} \approx \sqrt{0.2^2 + 0.003^2 + 0.008^2} \approx 0.2,$$

which indicates that the uncertainty of F_{CO2} is approximately 20% and determined mostly by the uncertainty of k (Wanninkhof, 2014).

3. Results

3.1. Observations of Full Record Data

Atmospheric and oceanographic observations made at the BOBOA mooring site reveal the SST had significant synoptic variabilities, with a large seasonal temperature cycle during the 39-month period between November 2013 and January 2017 (Figure 2a). The range of the SST seasonal cycle was about 4 °C, which varied from a minimum monthly mean of 26.9 °C in February to a maximum monthly mean of 30.7 °C in May (Figure 2b). The observed SSS at this site during the study period also had noticeable temporal variability with relatively large changes in December 2013 and September 2016 (Figure 2a), due mainly to heavy rainfalls in the region (data not shown). No obvious seasonal salinity cycle was observed at this mooring site during the 39-month period (Figure 2b). The daily observations of wind speeds had very high temporal variability

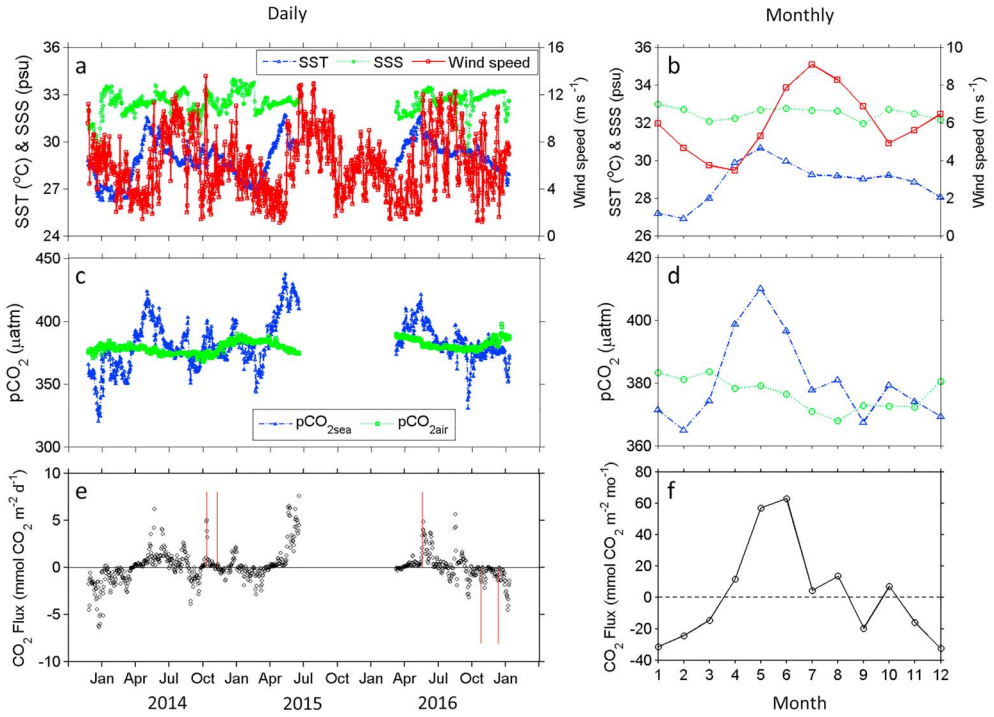

Figure 2. Observed daily time series of (a) SST, SSS, and wind speed; (b) pCO_{2sea}, pCO_{2air}, and pH; and (c) F_{CO2} at the BOBOA mooring site during the period from November 2013 to January 2017. Right panels show the monthly mean time series averaged from three-hourly observations shown in left panels. The red vertical lines in Figure 2e represent five TCs chosen for this study. BOBOA = Bay of Bengal Ocean Acidification; SST = sea surface temperature; SSS = sea surface salinity.

(Figure 2a) and a significant seasonal cycle during the study period, with a monthly mean minimum of about 3.5 m/s in the premonsoon and a monthly mean maximum of about 9.1 m/s during the monsoon (Figure 2b).

The daily observations of pCO_{2sea} (320–438 µatm) at the BOBOA mooring site had relatively large temporal variability, while the daily observations of pCO_{2air} had relatively small temporal variability and less than 6% during the study period (Figure 2c). The range of the observed seasonal cycle in pCO_{2sea} was about 45 µatm, which varied from a minimum of about 365 µatm in February to 410 µatm in May (Figure 2d). The high pCO_{2sea} in April–June was due mainly to high SSTs driven by strong solar radiations and weak winds. The low pCO_{2sea} in December–February was due mainly to low SSTs associated with weak solar radiations. The very low pCO_{2sea} on 20–25 February 2015, however, was probably due to the low SST and low salinity generated by the ocean circulation. The extremely low values of pCO_{2sea} on 17–26 December 2013 and also on 16–25 September 2016 were due most likely to the low salinity (heavy precipitation and low wind speeds) in the study region. The observed pCO_{2sea} decreased significantly from 403 µatm on 20 August 2014 to 351 µatm on 27 August 2014 (Figure 2c), which was due mainly to the low salinity generated by the heavy precipitation. Another large value of pCO_{2sea} in October 2014 was due to the passage of TC Hudhud. Overall, the monthly mean pCO_{2sea} had the highly similar seasonal pattern as the monthly mean SST. Similarly, large temporal variability of the daily F_{CO2} was observed at this mooring site during the study period (Figure 2e). Since the magnitude of F_{CO2} depends on the wind speed and the difference between pCO_{2sea} and pCO_{2air}, the observed maximum F_{CO2} of about 7.57 mmol CO_2 m^{-2} day^{-1} occurred when the observed winds and pCO_{2sea} reached a high value on 18 June 2015. Figure 2f demonstrates that the BOBOA mooring site was characterized by a CO_2 sink from September to March (except for October) and a CO_2 source from April to August. In comparing with the CO_2 sink in September and November, the opposite CO_2 source in October was affected by TC Hudhud on 8–11 October 2014, which is the motivation of our study to investigate the effect of TCs on the air-sea CO_2 exchanges in the BoB. The nonzero annual mean of F_{CO2} shown in Figure 2f indicates that this location had a weak net source of 55.78 ± 11.16 mmol CO_2/m^2 averaged from

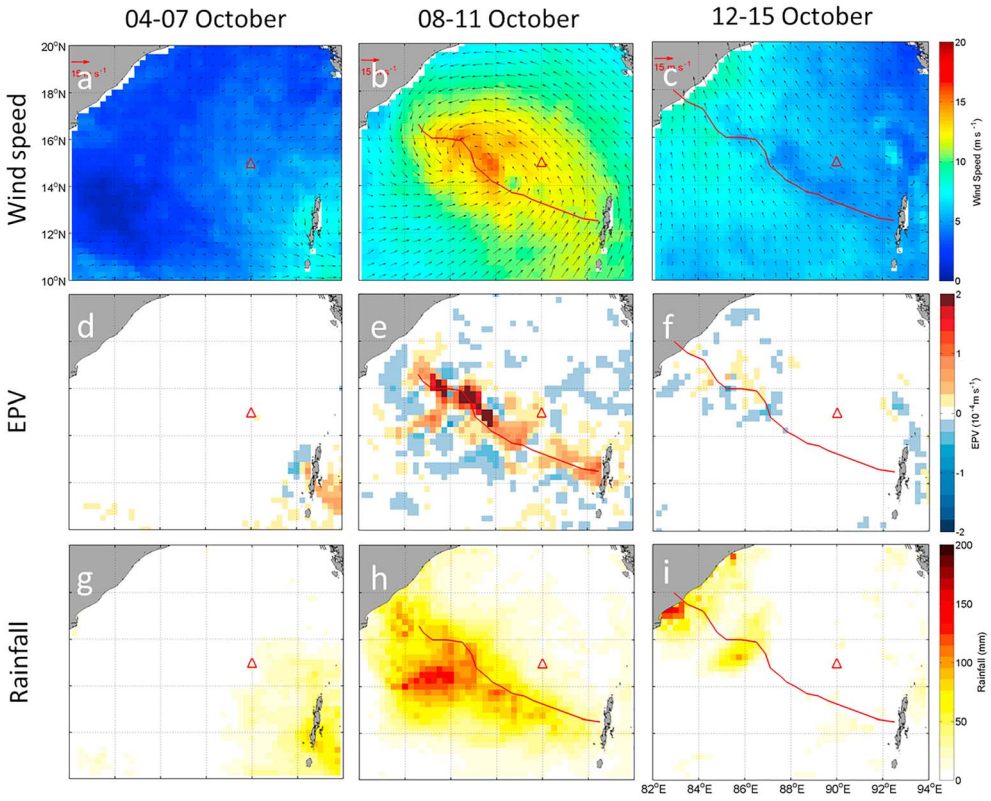

Figure 3. Satellite remote sensing data of 4-day time-mean (a–c) surface wind velocities and speeds (m/s); (d–f) Ekman pumping velocities (EPV, m/s), and (g–i) precipitations (mm/day) in the Bay of Bengal during the period of 4–15 October 2014. Left, middle, and right columns present the remote satellite data before, during, and after the passage of TC Hudhud. Red lines represent the track of TC Hudhud, and red triangle represents the BOBOA mooring site. BOBOA = Bay of Bengal Ocean Acidification; TC = tropical cyclone.

51.39 ± 10.28 mmol CO_2/m^2 in the whole year of 2014 and 60.16 ± 12.03 mmol CO_2/m^2 over the entire moored time series.

3.2. Wind, EPV, and Precipitation Affected by TC Hudhud

TC Hudhud was the first TC passing through the central BoB during the study period. The storm was a Category 4 TC originating from a tropical depression in the central BoB on 8 October 2014 (Figure 1). Hudhud moved northwestward and left the study region on 12 October 2014. The wind speeds were weak and less than 5 m/s on 4–7 October 2014 (before the storm) over the most part of the BoB, except for relatively strong and about 8 m/s over the southeastern area of the BoB (Figure 3a). During the TC on 8–11 October, very strong winds ($>$ 10 m/s) prevailed over the entire BoB (Figure 3b). The intensity of wind speeds ($>$ 15 m/s) was strong along Hudhud's track and about 13 m/s around the BOBOA mooring buoy. The 4-day time-mean wind speeds were significantly weakened after the TC on 12–15 October (Figure 3c), with weak winds ($<$ 7 m/s) over the most part of the BoB and about 5 m/s around the BOBOA mooring site.

Distributions of the EPVs shown in Figure 3d indicate that the wind-induced upwelling before TC Hudhud was very weak over the most of the BoB, except for small values ($< 2.5 \times 10^{-5}$ m/s) over the southeastern area of the BoB. During the passage of TC Hudhud on 8–11 October 2014, by comparison, the large and positive EPVs ($> 2 \times 10^{-4}$ m/s) occurred along the TC track and over areas to the right of the TC track (Figure 3e). The large negative EPVs over several local areas shown in Figure 3e (areas with dark blue colors) indicate occurrence of intense wind-induced downwelling over these areas. After the TC, the EPVs weakened significantly and returned to the prestorm values (Figure 3f).

In addition to the intense winds, Hudhud also brought a significantly large amount of precipitations. Before the storm on 4–7 October, the 4-day time-mean precipitations were generally low over the most of the BoB

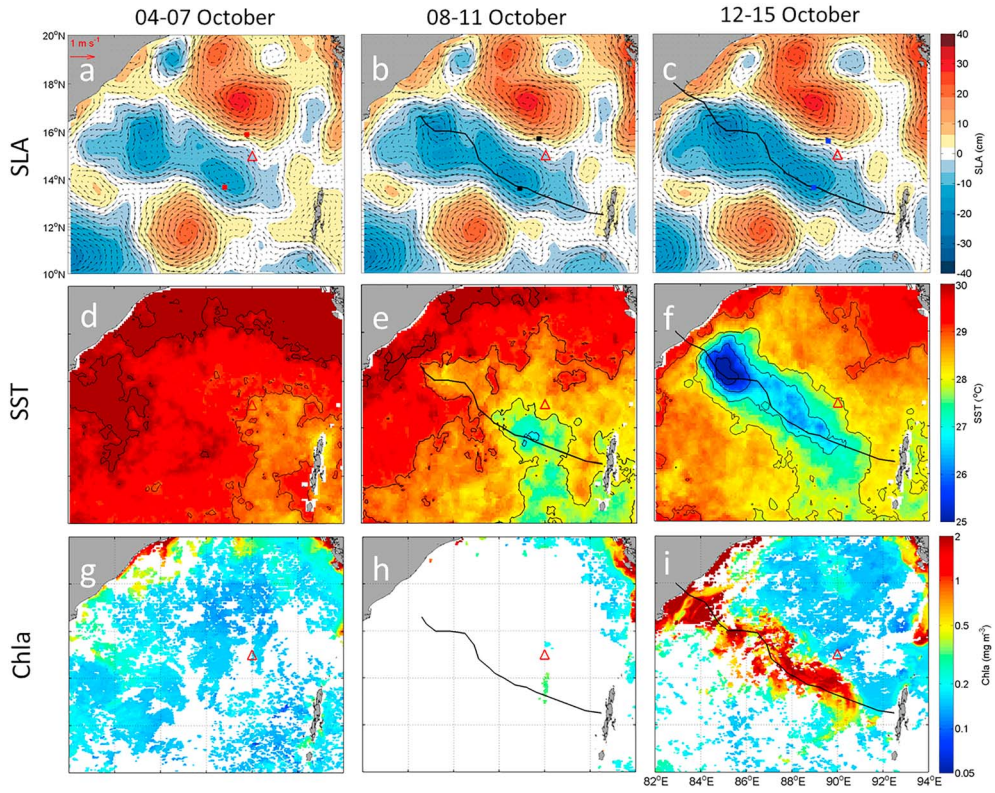

Figure 4. Satellite remote sensing data of 4-day time-mean (a–c) sea level anomalies (SLA, cm) and geostrophic currents at the sea surface (m/s), (d–f) sea surface temperature (SST, °C), and (g–i) chlorophyll *a* concentrations (Chla, mg/m^3) in the Bay of Bengal during the period of 4–15 October 2014. Left, middle, and right columns show satellite data before, during, and after the passage of TC Hudhud. Black lines represent the storm track of Hudhud, red triangles represent the BOBOA mooring site, and black solid squares represent the Argos position. The Chl*a* concentrations (h) before, (i) during, and (j) after Hudhud were averaged from 1 to 7, 8 to 13, and 14 to 18 October 2014, respectively. BOBOA = Bay of Bengal Ocean Acidification; TC = tropical cyclone.

(Figure 3g), except for slightly large precipitations of about 70 mm/day ahead of the storm over the southeastern area of the BoB. During the passage of Hudhud on 8–11 October, precipitations along the track of Hudhud increased up to 150 mm/day (Figure 3h). Figure 3h also shows that the heaviest rainfall was mainly left biased during Hudhud, which differs from the typical rainfall distribution for a TC (Lonfat et al., 2004). Usually, a large proportion of rainfall falls in advance of the storm center than after the passage of the storm, with the highest percentage falling in the right front quadrant (Lonfat et al., 2004), due to main factors such as the wind shear, SST, and moisture distribution. The rainfall was small after Hudhud on 12–15 October (Figure 3i).

3.3. Satellite-Derived SLA, SST, and Chla

The wind-pump effects (including vertical mixing and upwelling), the nonlinear dynamics of cold eddies, and the storm-induced currents are expected to affect the large-scale oceanic circulation in the BoB. Before Hudhud on 4–7 October, two large-size anticyclonic eddies (positive SLAs) occurred over the southwestern and northeastern areas of the BoB, and two attached cyclonic eddies (negative SLAs) occurred over the central area of the BoB (Figure 4a). These (western and eastern) cyclonic eddies emerged into one large-size cyclonic eddy during Hudhud's passage on 8–11 October (Figure 4b) and strengthened after Hudhud's passage on 12–15 October (Figure 4c). The strengths of the two anticyclonic eddies were similar over areas adjacent to the storm track during and after Hudhud. It should be noted that the BOBOA mooring buoy was located at the transition zone of the northeastern anticyclonic eddy and eastern cyclonic eddy, with the surface geostrophic currents to be about 0.3 m/s and approximately westward during the passage of Hudhud.

The MW_IR SST image on 4–7 October shown in Figure 4d features high SST (about 29 °C) over the whole BoB before the passage of Hudhud, except for the relatively lower SST over the southeastern area due most likely to the generation of Hudhud that took the heat energy from the ocean. During the passage of Hudhud, there was significant SST cooling over areas under the direct influence of the TC (Figure 4e). After Hudhud on 12–15 October, a significant SST cooling patch along the storm track with the maximum SST cooling of about 5 °C occurred over the area centered at about 86°E and 16°N (Figure 4f). The storm-induced SST cooling was only about 1 °C at the BOBOA mooring site due to its location of about 183 km away from the storm track.

The Chl*a* concentrations had significant spatial variability before and after the passage of Hudhud over the BoB (Figures 4g–4i). Before Hudhud on 1–7 October, the 7-day time-mean Chl*a* concentrations were generally low (< 0.2 mg/m^3) over the central and southern areas of the BoB (Figure 4g). During the passage of Hudhud 8–13 October, no valid data were available to derive Chl*a* concentrations due to the heavy cloud coverage (Figure 4h). Chacko (2017) reported, however, that a Chl*a* bloom along the storm track of Hudhud was observed by a bio-Argo float 2902114. After Hudhud on 14–18 October, the Chl*a* concentrations significantly increased to 0.5–4.0 mg/m^3 along the storm track (Figure 4i). The high Chl*a* concentrations were due to the combined effect of subsurface chlorophyll entrainment and nutrient injection (Chacko, 2017). At the BOBOA mooring site, the Chl*a* concentration was unchanged after 14 October.

3.4. Oceanic and Meteorological Conditions at the Mooring Site

As mentioned earlier, the storm center of TC Hudhud was about 183 km to the south of the BOBOA mooring site on 9 October 2014 and the storm moved northwestward during the period of 9–13 October with translational speeds of about 2.5 m/s (Figure 1b). As shown in Figure 5a, there was significant reduction in the short-wave radiation at the mooring site on 7–9 October due to heavy cloud covers associated with Hudhud. The observed long-wave radiations at the site were about 429 W/m^2 with small temporal variability during this period. The SLP at the mooring site decreased from about 1,010 hPa on 4 October (before the storm) to a minimum of about 999 hPa on 9 October and then gradually increased to the prestorm value of about 1,010 hPa (Figure 5b). The observed 10-m wind speeds at the mooring site were not strong and had large temporal variability with the mean value of about 3.7 m/s before the storm on 4–6 October (Figure 5b). The observed winds at the BOBOA mooring site increased significantly during the passage of Hudhud on 8–10 October and reached a maximum of about 13.6 m/s on 9 October. The observed winds then gradually decreased to light winds after the storm on 13–15 October.

The observed SST at the BOBOA mooring site demonstrates the storm-induced SST cooling associated with TC Hudhud. The observed SST at this site was about 29.4 ± 0.2 °C with significant temporal variability before the storm on 4–7 October and decreased to 28.6 ± 0.3 °C during the passage of the storm on 8–11 October 2014 (Figure 5c). The SST remained to be about 28.6 ± 0.3 °C after the storm on 12–15 October. The maximum observed SST cooling was more than 1 °C at the BOBOA mooring site. It should be noted that, on 6 October and 14–15 October, large diurnal SST signals occurred with a maximum at 12:17–14:17 UTC. During these days, the weather was fine and wind speeds were very low ($<$4 m/s).

The observed SSS at the BOBOA mooring site before the TC was relatively low and nearly constant (32.3 ± 0.1 psu) on 5 October before the storm (Figure 5c). During the passage of Hudhud on 9–10 October, the observed SSS increased to 32.7 psu, indicating that the surface waters were affected by subsurface waters with high salinity. The small salinity fluctuation on 5 October was associated mainly with heavy precipitations (~143 mm) and slightly low wind speeds ($<$5 m/s) on 4 October (Figure 5d). The small salinity fluctuation on 10 October was caused mainly by light precipitations (~60 mm) on that day.

3.5. pCO_{2sea} Variations and Air-Sea CO_2 Flux

The in situ observations at the BOBOA mooring site revealed significant variations in pCO_{2sea} (387.5 ± 8.6 μatm) associated with the passage of TC Hudhud (Figure 5e). Prior to TC Hudhud, the ocean waters around the BOBOA mooring site were a small source of CO_2 to the atmosphere with the mean ΔpCO_2 values of 8.1 μatm. The variation of pCO_{2sea} 379.7 ± 3.9 μatm was small with the maximum pCO_{2sea} occurring at the highest temperature and the minimum pCO_{2sea} occurring at the heavy precipitation period. During the passage of Hudhud between 8 and 11 October 2014, the pCO_{2sea} (388.1 ± 7.9 μatm)

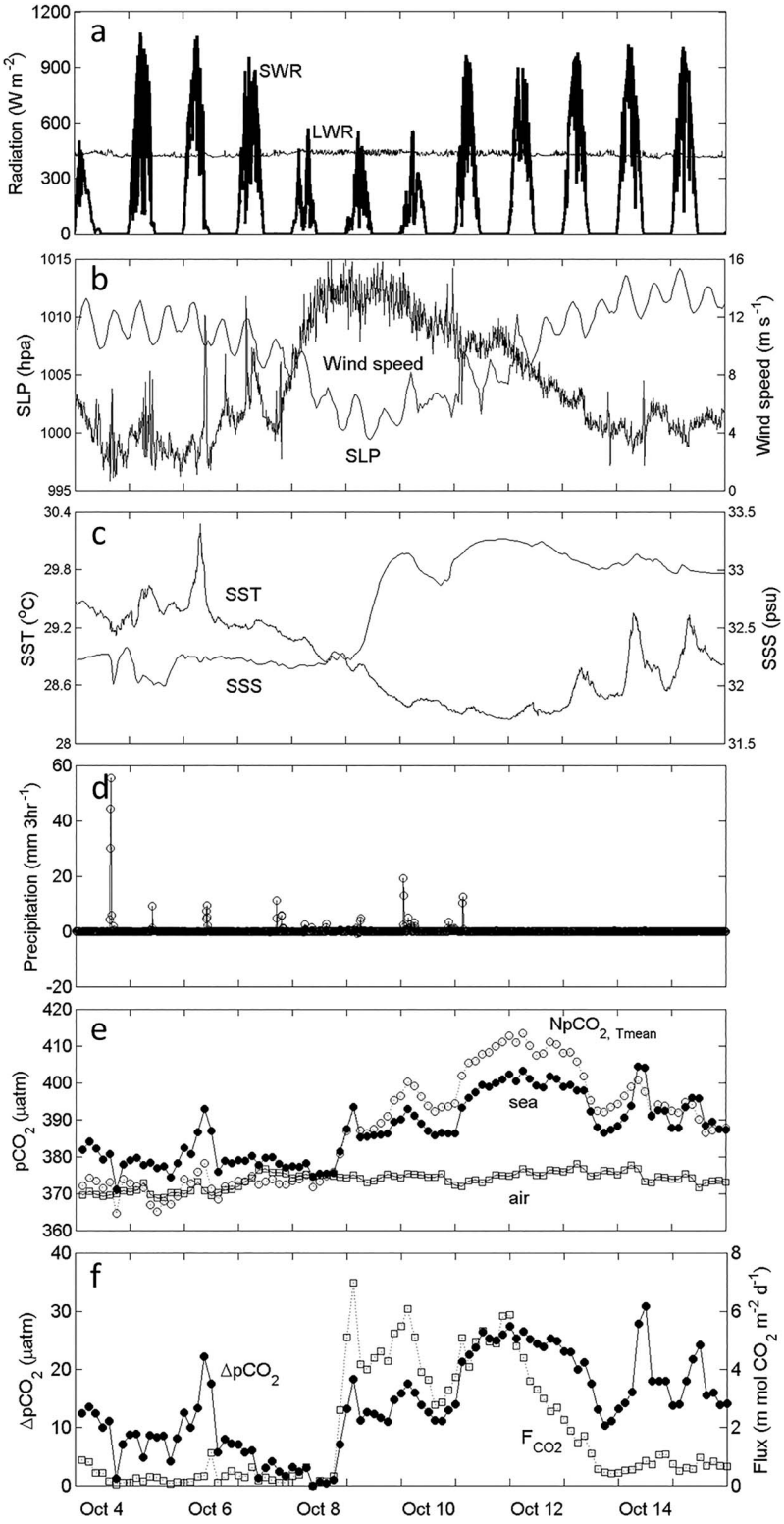

Figure 5. Observed time series of atmospheric and oceanographic conditions at the BOBOA mooring site on 4–15 October 2014. From top to bottom, (a) the downward shortwave radiation (bold line) and longwave radiation fluxes (thin line), (b) atmospheric pressure at the sea level and wind speed at 10-m height, (c) sea surface temperature (SST) and sea surface salinity (SSS), (d) precipitation, (e) pCO_{2air}, pCO_{2sea}, and $NpCO_{2,Tmean}$, and (f) ΔpCO_2 and F_{CO2}. Positive values of F_{CO2} indicate efflux of CO_2 from the ocean, and negative values indicate influx into the ocean. BOBOA = Bay of Bengal Ocean Acidification; SLP = sea level pressure.

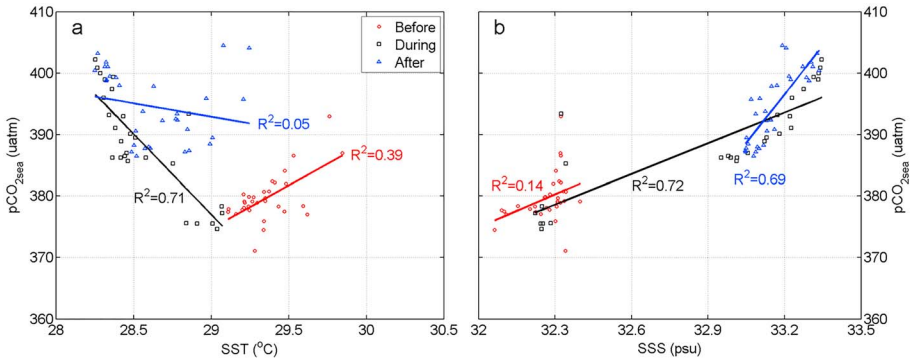

Figure 6. Scatterplots between different oceanographic variables measured at the sea surface: (a) SST versus pCO_{2sea} and (b) SSS versus pCO_{2sea} before (blue triangles), during (black boxes), and after (red circles) the passage of Hudhud for the period of 4–15 October 2014. SSS = sea surface salinity; SST = sea surface temperature.

increased significantly with time, with the mean ΔpCO_2 value of 13.8 μatm. After the passage of Hudhud on 12–15 October, the pCO_{2sea} gradually increased to 404.5 μatm and then decreased to about 387 μatm with the mean value of about 394.5 ± 5.8 μatm. It should be noted that the pCO_{2air} was approximately constant on 4–15 October with the mean value of about 373.6 ± 2.3 μatm.

To examine the effects of properties other than water temperature on the variation of pCO_{2sea}, pCO_{2sea} normalized to the mean temperature ($NpCO_{2,Tmean}$) is developed by Takahashi et al. (2002),

$$NpCO_{2,T\mathrm{mean}} = pCO_{2sea} \times \exp(0.0423(T_{\mathrm{mean}} - T_{\mathrm{obs}})), \quad (6)$$

where T is SST in °C, and the subscripts *mean* and *obs* indicate the temperature averaged and in situ values on 4–14 October. The $NpCO_{2,Tmean}$ increased significantly at the time of minimum SLP and persisted over more than 6 days (Figure 5e). The $NpCO_{2,Tmean}$ showed similar variations with the pCO_{2sea} on late 8 October and early 9 October, and about 8 μatm higher than the pCO_{2sea} in the following 4 days. The $NpCO_{2,\ Tmean}$ changed from lower than the pCO_{2sea} before the TC to higher than the pCO_{2sea} during the TC, synchronized decrease in SST approximately with the increase in SSS, indicating much DIC supply due to vertical mixing corresponding to the entrainment at the base of the top mixed layer. The $NpCO_{2,Tmean}$ gradually decreased from the highest value on 12 October to the same level as the pCO_{2sea} after 14 October, combined with high pCO_{2sea} suggesting DIC supply played a larger role than possible occurrence of biological DIC consumption in determining pCO_{2sea}.

The values of ΔpCO_2 determine the directions of F_{CO2}. Prior to Hudhud, the surface waters around the BOBOA mooring site were oversaturated with the averaged F_{CO2} value of about 0.30 ± 0.25 mmol CO_2 m^{-2} day^{-1} (Figure 5f). During the passage of Hudhud, the averaged F_{CO2} value was about 3.77 ± 1.97 mmol $CO_2 m^{-2} day^{-1}$ with a maximum value raised to about 6.97 mmol CO_2 m^{-2} day^{-1} on 9 October at 00:17 UTC, due to the strong wind effect. Concurrent with the wind speeds decreasing to the prestorm values, the F_{CO2} gradually decreased to the prestorm values, with the averaged value of about 1.44 ± 1.23 mmol CO_2 m^{-2} day^{-1} after the passage of Hudhud. The CO_2 efflux enhanced by TC Hudhud was about 18.49 ± 3.70 mmol CO_2/m^2 in 8 days.

The SST-pCO_{2sea} and SSS-pCO_{2sea} diagrams (Figure 6) were used to examine the dependence of pCO_{2sea} on the SST and SSS. Before the passage of Hudhud in the BoB, pCO_{2sea} was moderately correlated to SST with a positive correlation coefficient value of $R^2 \approx 0.39$ and weakly correlated to SSS with a positive value of $R^2 \approx 0.14$ (Figure 6). This indicates that both temperature and salinity played some but nondominant role in determining pCO_{2sea} before the storm. During the passage of Hudhud, pCO_{2sea} was significantly correlated to SST with a negative value of $R^2 \approx 0.71$ and also significantly correlated to SSS with a positive value of $R^2 \approx 0.72$. After Hudhud, pCO_{2sea} was strongly and positively correlated with SSS with a large value of $R^2 \approx 0.69$ but weakly correlated to SST with a small value of $R^2 \approx 0.05$. The results indicate that physical processes played a much more important role than the biological DIC consumption in affecting the change in pCO_{2sea} during and after Hudhud than before the storm.

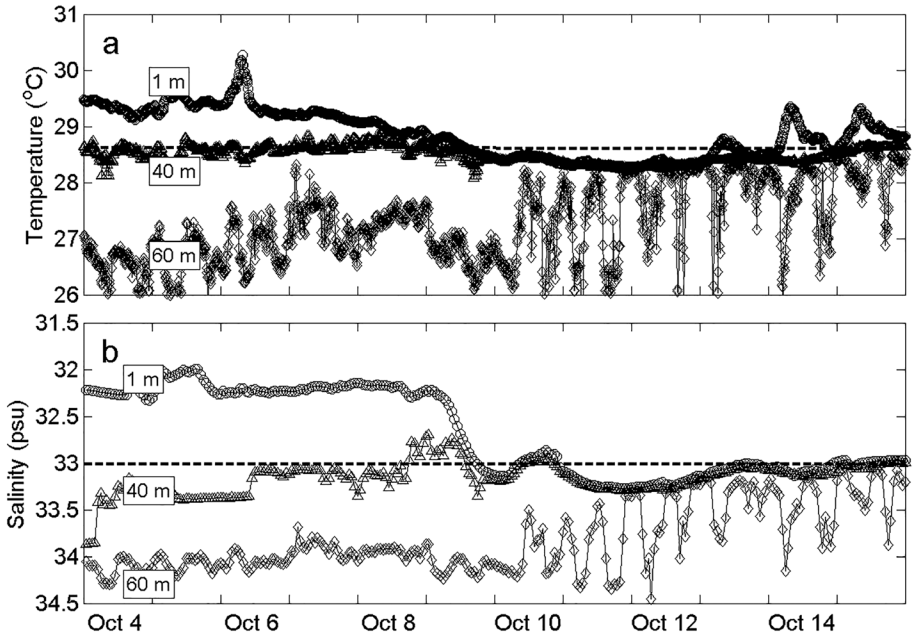

Figure 7. Observed hourly time series of (a) water temperature and (b) salinity at depths of 1, 40, and 60 m of the BOBOA mooring site for the period of 4–15 October 2014. BOBOA = Bay of Bengal Ocean Acidification.

3.6. Vertical Structures at the Mooring Site

Figure 7 presents hourly time series of observed hydrography at three different depths in the upper water column at the BOBOA mooring site. Before the passage of Hudhud on 4–7 October 2014, the observed water temperature and salinity were vertically stratified at the mooring site. During the passage of the storm on 8–9 October, the observed water temperature and salinity at 40 m were nearly equal to those at 1 m, indicating vertically uniform water mass in the top 40 m due most likely to the intense vertical mixing caused by strong winds associated with TC Hudhud on these days (Figures 3 and 5). After the storm on 12–15 October, the observed temperature (salinity) at 1 and 40 m gradually increased (decreased) with time (Figure 7).

It should be noted that a TC (or typhoon) can generate not only strong vertical mixing but also strong upwelling (Sheng et al., 2006; Song & Tang, 2017). The latter could also lead to vertically uniform distributions of water temperature and salinity in the upper water column if the storm-induced upwelling lasts long enough for subsurface waters to reach the sea surface. The observed temperature at 60 m was generally cooler than the temperature at 40 m during the passage of Hudhud (Figure 7a), Furthermore, the running mean of the observed temperature at 60 m during the passage of the storm was about 27.9 °C, which was about 1.1 °C warmer than the observed temperature at the same depth before the storm. Hence, the storm-induced upwelling played only a very minor role for the vertically uniform water mass in the top 40 m and reduced vertical stratifications between 40 and 60 m at the BOBOA mooring site during and after the passage of Hudhud. The observed water temperature and salinity at 60 m had very large temporal fluctuations during and after the passage of Hudhud (Figure 7). The exact reason for these large temporal fluctuations at 60 m is unknown. One plausible explanation is that temperature and salinity sensors at 60 m were near the interface of two different water masses after 9 October, and the sensors made hydrographic measurements of these two different masses once the interface had some vertical movements.

Figure 8a presents vertical profiles of 4-day time-mean temperature and salinity observations at the BOBOA mooring site. The observed temperature (salinity) was cooler (higher) than the counterpart before the storm in the upper 40 m. At depths between 40 and 100 m, the observed temperature (salinity) was relatively warmer (lower) than the counterpart before the storm. Below 100 m the observed hydrography remained unchanged during the passage of Hudhud. The noticeable temporal changes in the observed hydrography in the top 100 m were caused by the strong vertical mixing induced by Hudhud. Furthermore, TC Hudhud also enhanced the MLD from 20 to 60 m and deepened the ILD from 60 to 80 m, while the thickness of the BL was reduced from 40 to 20 m.

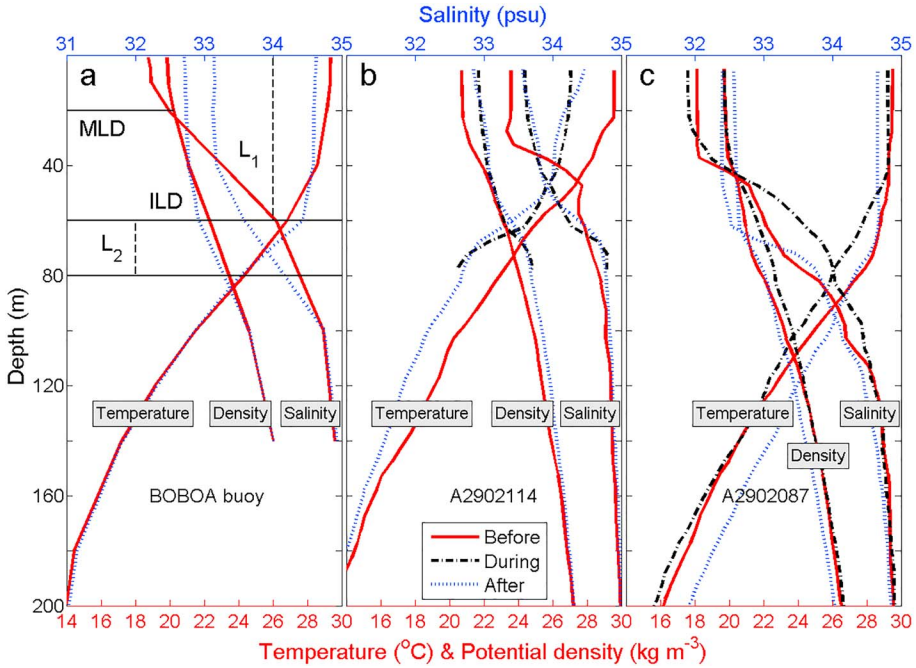

Figure 8. Vertical profiles of 4-day time-mean temperature and salinity observations and calculated potential density before, during, and after the passage of TC Hudhud at (a) BOBOA mooring site averaged from 4 to 7, 8 to 11, and 12 to 15 October 2014; (b) Argo float 2902114 from 5, 10, and 15 October and (c) Argo float 2902087 from 4, 9, and 14 October. ILD is calculated as the depth where the water temperature decreases by 1 °C from its surface value. MLD is defined as the depth where the potential density increases by 0.125 kg/m^3 from its surface value. L_1 is the upper of ILD, and L_2 is the layer between ILD and the depth at which water temperature is cooler by 3 °C than the SST. BOBOA = Bay of Bengal Ocean Acidification; SST = sea surface temperature; MLD = mixed layer depth; ILD = the depth of the top of the thermocline.

3.7. Vertical Profiles at Argo Floats

Argo float 2902114 was located inside the cyclonic eddy waters and hit directly by Hudhud (Figures 4a–4c). Vertical profiles of observed hydrography at this Argo float (Figure 8b) indicate that the ILD (MLD) for the cyclonic eddy waters was about 32.6 m (37.6 m) before the passage of Hudhud and increased (decreased) to 47.6 m (32.6 m) during the storm on 10 October and decreased to 17.4 m (22.4 m) after the storm on 15 October 2014. The BL did not appear during the entire study period. The decreased temperature in the upper 200 m and increased salinity between 70 and 100 m at this float site indicate very strong upwelling caused most likely by TC Hudhud. The increased salinity in the upper 40 m and decreased salinity at intermediate depths between 40 and 70 m indicate a very strong vertical mixing induced by Hudhud.

Argo float 2902087 was located at the edge of the anticyclonic eddy (Figures 4a–4c) during the period of 4–15 October. Figure 8c demonstrates that the thickness of the BL is about 45 m before Hudhud at this float site. The BL thickness was thinner and about 30 and 40 m during and after Hudhud, respectively, indicating a very strong mixing caused by Hudhud. During the passage of Hudhud, a slightly low SSS occurred due mainly to heavy precipitations on 8–11 October (Figure 5). The salinity increased in the upper 40 m and decreased between 40 and 70 m, showing the very strong mixing. The increased temperature and decreased salinity below 90 m were due most likely to the moment of the Argo float into the anticyclonic eddy, within which strong downwelling was expected.

4. Discussion

4.1. Enhanced pCO_{2sea} Due to the Passage of TC Hudhud

As discussed above, the 4-day time-mean pCO_{2sea} at the BOBOA mooring site increased of about 8.4 ± 11.8 and 14.8 ± 9.7 μatm, respectively, during and after the passage of TC Hudhud from its prestorm value (Figure 5e). Furthermore, the cross-correlation coefficient between pCO_{2sea} and SST changed from a

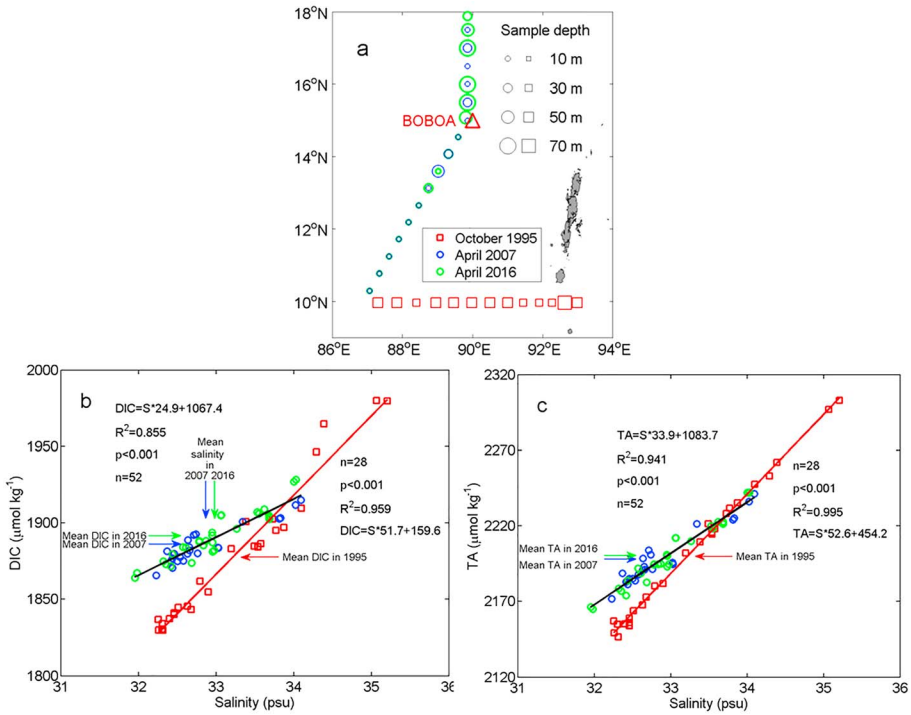

Figure 9. (a) Map of the Bay of Bengal showing the sample stations employed in this study, of which size represents the sample depth, (b) DIC versus salinity, and (c) TA versus salinity in the thermocline layer (the depth at which temperature decreases by 1 °C from the surface temperature). The data collected during a WOCE cruise in October 1995 (postmonsoon; red squares), and two GO-SHIP cruises in April 2007 (premonsoon; blue circles) and April 2016 (premonsoon; green circles) and can be downloaded from the Climate Variability and Predictability and Carbon Hydrographic Data Office (http://cchdo.ucsd.edu/). DIC = dissolved inorganic carbon; TA = total alkalinity; WOCE = World Ocean Circulation Experiment; GO-SHIP = Global Ocean Ship-based Hydrographic Investigations Program.

moderately positive value before the storm to a significantly negative value during the storm. The cross-correlation coefficient between pCO_{2sea} and SSS changed from a marginally positive value before the storm to a significantly positive value during the storm (Figure 6). The $NpCO_{2,Tmean}$ changed from lower than the value of pCO_{2sea} before the storm to higher than pCO_{2sea} during the storm and then gradually decreased to the same level as the pCO_{2sea} after the storm (Figure 5e). These results indicate that relatively cool, high salinity and CO_2-rich subsurface waters were mixed and upwelled to the surface due to the wind-pump effects (Song & Tang, 2017; Ye, Kalhoro, et al., 2017; Ye, Sheng, et al., 2017). A strong negative relationship between pCO_{2sea} and SST (Ye, Sheng, et al., 2017) and a significantly positive relationship between pCO_{2sea} and SSS were also observed in the South China Sea after passages of typhoons (Sun et al., 2014; Ye, Sheng, et al., 2017).

The significantly negative cross correlation between pCO_{2sea} and SST (Figure 6a) during TC Hudhud motivates us to examine the vertical inorganic carbon conditions in the BoB during the postmonsoon. The observational program known as the World Ocean Circulation Experiment (WOCE, Sabine et al., 2002) collected various types of in situ oceanographic data that can be used to generate distributions of DIC and TA in the world's oceans. During the postmonsoon in October 1995, a WOCE cruise was conducted in the BoB (Figure 9a). (The WOCE observational data were downloaded from the website for the Climate Variability and Predictability and Carbon Hydrographic Data Office at http://cchdo.ucsd.edu/). Regional relationships between salinity and DIC and TA were determined using WOCE samples collected in the upper layer of ILD between 10–18°N and 87–93°E (Fassbender et al., 2017). The correlation analysis of the WOCE data yields significantly positive cross correlations of DICs (DIC = salinity × 51.7 + 159.6; $R^2 \approx 0.995$, $P < 0.001$) and TAs (TA = Salinity × 52.6 + 454.2, $R^2 \approx 0.959$, $P < 0.001$) with salinity in the upper layer of the ILD, with a standard deviation of about ±9.2 and ±3.2 μmol/kg, respectively (Figures 9b and 9c). It was suggested that TA is not affected by anthropogenic CO_2 but only weakly altered by the

uptake/release of protons associated with reduction/oxidation (Sabine et al., 2002). As shown in Figure 5c, the SSS increased from a prestorm value of about 32.3 psu to a poststorm value of about 33.2 psu during TC Hudhud in October 2014, and the TAs increased from a prestorm value of about 2,153.2 ± 9.2 μmol/kg to a poststorm value of about 2200.5 ± 9.2 μmol/kg estimated using the linear relationship between TA and salinity shown in Figure 9c. Previous studies also suggested that DIC is strongly influenced by the biological pump and also affected by the air-sea exchange and input of anthropogenic CO_2 (Sabine et al., 2002). The increasing DIC due to elevated anthropogenic inputs, such as at the station ALOHA (Keeling et al., 2004) and North Atlantic Ocean near Bermuda (Bates, 2007), was reported in the literature. We calculated the long-term increasing sDIC (normalized to a salinity of 35.0) trend in the upper layer of ILD of the BoB based on two Global Ocean Ship-based Hydrographic Investigations Program cruises (http://cchdo.ucsd.edu/) conducted on, respectively, 23–27 April 2007 and 20–24 April 2016 (Figure 9a). The increasing sDIC trend is about −0.15 ± 0.64 μmol·kg^{-1}·year^{-1} (standard error). The DICs before and after Hudhud were about 1826.7 ± 15.2 and 1873.2 ± 15.2 μmol/kg estimated from the linear relationship between DIC and salinity shown in Figure 9b and the increasing sDIC trend, respectively. The thermodynamic relationships suggested by Takahashi et al. (1993) were used:

$$\mathrm{d}p\mathrm{CO}_2 = (\partial p\mathrm{CO}_2/\partial T)\mathrm{d}T + (\partial p\mathrm{CO}_2/\partial \mathrm{DIC})\mathrm{dDIC} + (\partial p\mathrm{CO}_2/\partial \mathrm{TA})\mathrm{dTA} + (\partial p\mathrm{CO}_2/\partial \mathrm{S})\mathrm{d}S \quad , \tag{7}$$

where T represents SST and S represents SSS. The values of the four partial differential terms on the right-hand side of equation (7) for tropical waters were used:

$$(\partial pCO_2/\partial T)/p\mathrm{CO}_2 = 0.0423°\mathrm{C}^{-1} \tag{8}$$

$$(\partial p\mathrm{CO}_2/\partial \mathrm{DIC})(\mathrm{DIC}/p\mathrm{CO}_2) = 8 \tag{9}$$

$$(\partial p\mathrm{CO}_2/\partial \mathrm{TA})(\mathrm{TA}/p\mathrm{CO}_2) = -7.4 \tag{10}$$

$$(\partial p\mathrm{CO}_2/\partial S)(S/p\mathrm{CO}_2) = 0.93. \tag{11}$$

Based on the SST decrease from a prestorm value of 29.4 ± 0.2 °C to a poststorm value of 28.6 ± 0.3 °C during TC Hudhud and equation (8), the storm-induced SST cooling leads to a decrease of −12.8 ± 5.3 μatm (Table 2). The increase in surface DICs and TAs leads to 77.4 ± 0.6 and −61.8 ± 0.1 μatm changes in pCO_{2sea}, respectively. The salinity change generated by storm-induced vertical mixing leads to an increase of 9.8 ± 1.5 μatm in pCO_{2sea}.

The pCO_{2sea} change is determined mostly by the phytoplankton photosynthesis processes, air-sea CO_2 fluxes and coupled DIC, TA, temperature, and salinity change. Water temperature was found to be the key factor for decreasing pCO_{2sea} during Hurricanes Felix and Frances in the North Atlantic Ocean (Bates et al., 1998; Huang & Imberger, 2010), and also during Typhoons Tina and Winnie in the East China Sea (Nemoto et al., 2009; Wada et al., 2011). Meanwhile, the DIC was found to be the crucial factor for increasing pCO_{2sea} after the passage of typhoons in the South China Sea (Sun et al., 2014; Ye, Sheng, et al., 2017). The precipitation accompanied by a TC can dilute the salinity in the surface ocean waters, which can decrease the pCO_{2sea} (Sun et al., 2014). The observed time series of temperature and salinity shown in Figure 7 indicate that the storm-induced strong vertical mixing *uplifted* subsurface waters (at depths up to 60 m) to the surface layer at the BOBOA mooring site where the depth of the subsurface chlorophyll maximum was about 45–55 m (Chacko, 2017). This indicates that high Chl*a* concentrations occurred in the BOBOA waters, due mainly to the subsurface waters of high Chl*a* concentrations mixed to the surface layer waters although satellite Chl*a* images were not available during the passage of Hudhud on 8–13 October 2014. The very small change in Chl*a* concentrations in the BOBOA waters (comparing Figures 4g with 4i) indicates that the phytoplankton photosynthesis processes may not have a great impact on pCO_{2sea} after 14 October. High pCO_{2sea} within a cyclonic eddy core indicates that the upwelling of CO_2-rich subsurface water was the key factor, while low pCO_{2sea} within the eddy edge was due to the combination of biological uptake, physical upwelling, and thermodynamics (Chen et al.,

Table 2
The pCO_{2sea} Variations Derived by the Change of SST, SSS, DIC, and TA Based on Equations ((8)–(11)), and Air-Sea CO_2 Flux Based on Equations ((12)–(14))

Tropical cyclone	dSST	dSSS	dDIC	dTA	dF_{CO2}	Total
Hudhud	−12.8 ± 5.3	9.8 ± 1.5	77.4 ± 0.6	−61.8 ± 0.1	−0.9 ± 0.2	11.7 ± 7.6
Five	−8.6 ± 4.2	2.7 ± 3.5	21.4 ± 0.2	−17.1 ± 0.0	0.0 ± 0.0	−1.6 ± 7.9
Kyant	−4.7 ± 3.7	1.5 ± 0.9	11.7 ± 0.1	−9.3 ± 0.0	0.3 ± 0.0	−0.5 ± 4.6
Vardah	−1.9 ± 3.1	0.1 ± 0.6	0.8 ± 0.0	−0.7 ± 0.0	−0.1 ± 0.0	−1.5 ± 3.7
Roanu	−20.2 ± 6.2	9.5 ± 3.6	35.0 ± 0.3	−37.8 ± 0.1	−1.5 ± 0.3	−15.0 ± 10.4

Note. Uncertainties (±) represent 1 standard deviation. SST = sea surface temperature; TA = total alkalinity; SSS = sea surface salinity; DIC = dissolved inorganic carbon.

2007). The air-sea CO_2 fluxes on the pCO_{2sea} variability can be estimated as the change of DIC in the MLD (ΔDIC_{MLD}) and $\left[H_2CO_3^*\right]$ (Sarmiento & Gruber, 2006):

$$\Delta DIC_{MLD} = \Delta F_{CO2}/MLD_a/\rho_0 \tag{12}$$

$$\partial DIC_{MLD}/\partial\left[H_2CO_3^*\right] = 20 \tag{13}$$

$$\Delta pCO_{2MLD} = \left[H_2CO_3^*\right]/K_H \tag{14}$$

where $\left[H_2CO_3^*\right]$ is the sum of the aqueous CO_2 and the true carbonic acid (H_2CO_3), MLD_a is the MLD after the Hudhud set to 60 m. The estimated ΔDIC_{MLD} is about 0.3 μmol/kg, which decreases the pCO_{2sea} of about 0.5 ± 0.1 μatm based on equation (9). The pCO_{2sea} change in the MLD due to F_{CO2} (ΔpCO_{2MLD}) is about 0.4 ± 0.1 μatm. In total, the effect of air-sea CO_2 fluxes on the pCO_{2sea} is about −0.9 ± 0.2 μatm (Table 2), which is consistent with previous estimations (Chen et al., 2007; Turi et al., 2014). Therefore, the total increase of pCO_{2sea} generated by TC Hudhud is estimated to be about 11.7 ± 7.6 μatm, which is comparable to the observed increase in pCO_{2sea} of about 14.8 ± 9.7 μatm.

The pCO_{2sea} variations derived from the change of SST, SSS, DIC, TA, and air-sea CO_2 fluxes were examined during other four TCs (i.e., TCs Five, Kyant, Vardah, and Roanu) between November 2014 and December 2016 (Table 2). Our results demonstrate that these four storms caused small SST cooling (−0.2 to −0.8 °C) during the postmonsoon and strong SST cooling (−1.2 °C) during the premonsoon (Table 1). Overall, the TC-induced SST cooling during the postmonsoon was much weaker than the counterpart during the premonsoon. This indicates that the TC-induced mixing did not reduce the SST during the postmonsoon, which is consistent with previous findings (Neetu et al., 2012; Sengupta et al., 2008). Furthermore, a wide range in increases of pCO_{2sea} (+1.0 to +14.8 μatm) induced by these storms occurred during the postmonsoon. By comparison, a significant decrease of −14.0 μatm in pCO_{2sea} was observed during the premonsoon. The Roanu-induced SST cooling led to a decrease of −20.2 ± 6.2 μatm (Table 2), which is consistent with previous findings (Bates et al., 1998; Huang & Imberger, 2010; Wada et al., 2011).

The above-mentioned different responses motivate us to examine the inorganic carbon conditions during the premonsoon and postmonsoon. Figure 10 presents vertical profiles of DICs, TAs, and DIC/TA before and after the passage of TC Hudhud at the BOBOA mooring site. The DICs, TAs, and DIC/TA were relatively lower than the counterpart in the upper 40 m and relatively higher than the counterpart at depths between 40 and 100 m before the storm. The DIC/TA values of about 0.849 ± 0.008 in L_1 and 0.896 ± 0.027 in L_2 were observed before the storm. The large ΔDIC/TA value of about 0.047 ± 0.028 corresponds to an increase of pCO_{2sea} of about 30 ± 15 μatm, assuming that the waters in L_2 were uplifted to L_1 (Goyet et al., 1993). The intense vertical mixing induced by TC Hudhud (Figures 7 and 8) uplifted some L_2 waters to the surface, which in turn increased the pCO_{2sea}. The ΔDIC/TA before other four TCs were also examined (Table 1). Large ΔDIC/TA (0.042 ± 0.027 to 0.048 ± 0.027) during the postmonsoon and small ΔDIC/TA (0.003 ± 0.014) during the premonsoon were observed. The reason for increases of pCO_{2sea} (+1.0 to +4.0 μatm) induced by other three storms lower than TC Hudhud during the postmonsoon is because of the weaker wind speeds during and/or deeper MLDs before the storm (Table 1). The small ΔDIC/TA value corresponds to a limited pCO_{2sea} increase

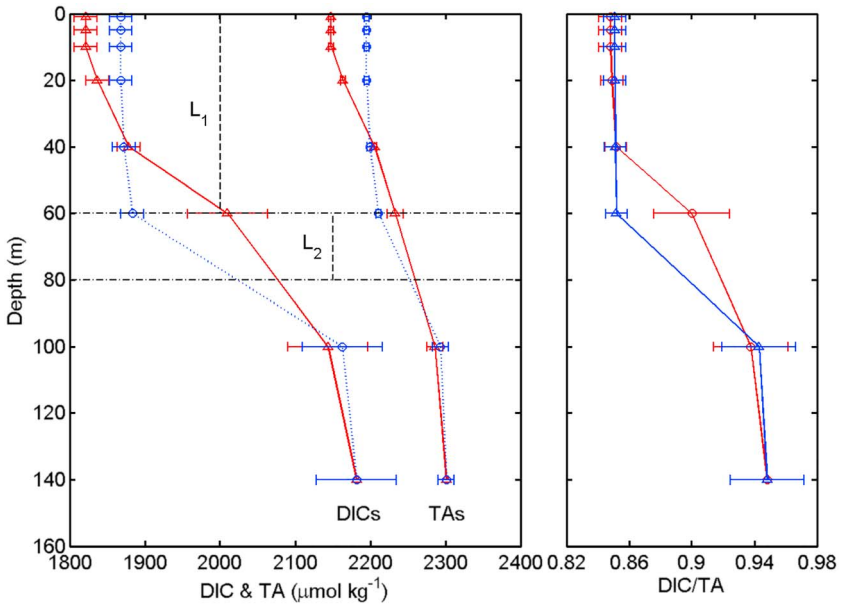

Figure 10. Vertical profiles of 4-day time-mean DICs, TAs (a), and DIC/TA (b) before (4–7 October 2014) and after (12–15 October 2014) the passage of TC Hudhud at BOBOA mooring site. The concentrations of DIC and TA were derived from the DIC-salinity and TA-salinity relationships based on 28 samples in L_1 (DIC = 51.7 × salinity + 159.6, R^2 = 0.96, $P < 0.001$; TA = 52.6 × salinity + 454.2, R^2 = 0.995, $P < 0.001$) and 100 samples in the depth within the layer between ILD and 500 m (DIC = 215.3 × salinity − 5322.5, R^2 = 0.46, $P < 0.001$; TA = 82.9 × salinity − 587.9, R^2 = 0.76, $P < 0.001$). BOBOA = Bay of Bengal Ocean Acidification; DIC = dissolved inorganic carbon; TA = total alkalinity; TC = tropical cyclone; ILD = the depth of the top of the thermocline.

(Goyet et al., 1993), which in turn decreases the pCO_{2sea} during the premonsoon. A remarkably constant DIC/TA of about 0.85 in the surface waters of the BoB was reported by Goyet et al. (1999) and Sabine et al. (2002). A small difference (near zero) in DIC/TA between surface waters and subsurface waters at 100 m that was observed in the Atlantic Ocean at 66.00°W and 22.21°N (Huang & Imberger, 2010) confirmed our analysis presented above. It should be noted that significant changes in pCO_{2sea} of about −20 μatm, which was induced by other two TCs (i.e., Maarhtha on 14–17 April 2017 and Mora on 27–30 May 2017) during the premonsoon, were also estimated based on a simple calculation of the preliminary data (from the interactive plots of https://www.pmel.noaa.gov/co2/story/BOBOA).

4.2. Effects of TCs on Local F_{CO2}

The F_{CO2} enhanced by TC Hudhud was estimated to be about 18.49 ± 3.70 mmol CO_2/m^2. Considering the annual F_{CO2} of 55.78 ± 11.16 mmol CO_2/m^2 for the BOBOA water (see section 3.1), the impact of the passage of TC Hudhud on the local CO_2 exchange was very significant. The impacts of other four TCs on the water properties and CO_2 exchange were summarized in Figure 11 and Table 1. During the postmonsoon in November 2014, the ocean waters were close to equilibrium with a weak influx before the passage of TC Five (Figure 11a). The small changes in SST, SSS, and F_{CO2} resulted from the moderate wind speeds (with the mean of about 7.2 m/s) and relatively shallow MLD during TC Five (Table 1). In October–December 2016, the ocean waters were undersaturated with the averaged F_{CO2} about −0.23 and −0.82 mmol CO_2 m^{-2} day^{-1} before passages of TCs Kyant and Vardah, respectively (Figures 11b and 11c). During TC Kyant, the wind speeds were moderate of about 8.5 m/s and the MLD was relatively deep, with a slightly decrease in SST and slightly increase in SSS. The moderately enhanced CO_2 influx (−3.86 ± 0.77 mmol CO_2/m^2) by TC Kyant was due to the combination of the wind effect during TC and wind-pump effects after Kyant. By comparison, small changes in SST and SSS induced by TC Vardah were due to the low SST and high SSS before Vardah, although the wind speeds (10.6 m/s) were relatively strong. A small change in F_{CO2} (1.22 ± 0.24 mmol CO_2/m^2) was due to the counteraction of the wind effect during Vardah and the wind-pump effects after Vardah. It should be noted that the TC-induced F_{CO2} changes

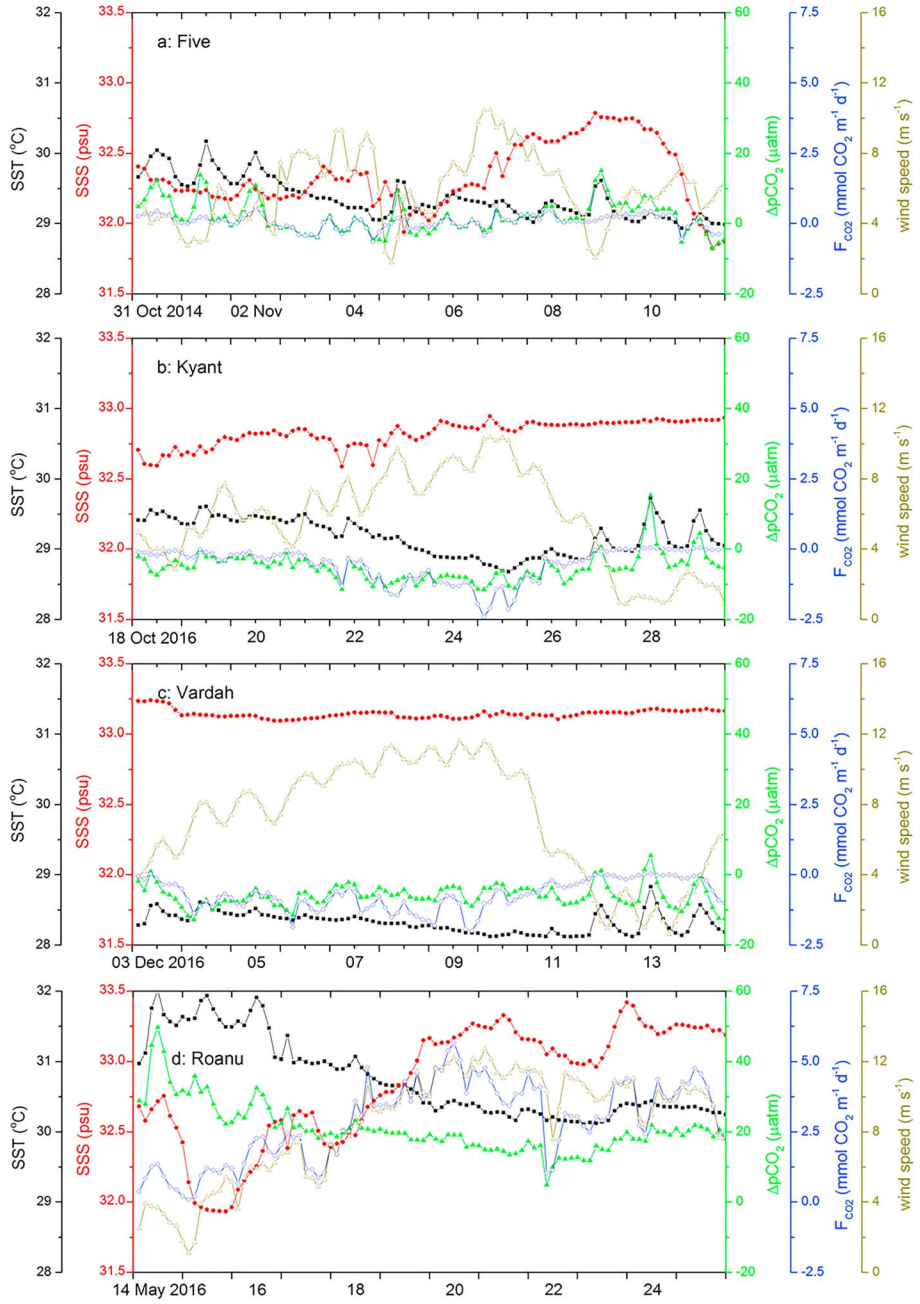

Figure 11. Observed 3-hourly time series of SST, SSS, wind speed, ΔpCO_2, and F_{CO2} before, during, and after TC (a) Five, (b) Kyant, (c) Vardah, and (d) Roanu. SSS = sea surface salinity; SST = sea surface temperature; TC = tropical cyclone.

during the postmonsoon discussed above differ from the results reported by Levy et al. (2012), who reported that TCs increase the CO_2 influx in undersaturated areas. The average enhancement of F_{CO2} from four TCs during the postmonsoon was about 3.91 ± 0.78 mmol CO_2/m^2 in 8 days.

During the premonsoon, the SST of about 31.4 °C and the SSS of about 32.4 were observed (Figure 11d). The combination of low wind speeds of 4.7 ± 1.7 m/s and high ΔpCO_2 of 28.0 ± 7.6 μatm resulted in a small CO_2 efflux (1.27 ± 0.69 mmol CO_2 m^{-2} day^{-1}). During and after TC Roanu, a significant decrease in SST and a large increase in SSS were observed due to high wind speeds (10.5 m/s) and relatively shallow MLD (Table 1). The averaged ΔpCO_2 was decreased to 18.0 ± 2.5 and 16.8 ± 4.0 μatm, respectively, which were conditions favorable for the continued CO_2 efflux. The F_{CO2} during and after TC Roanu was 3.95 ± 0.86 and 3.35 ± 0.96 mmol

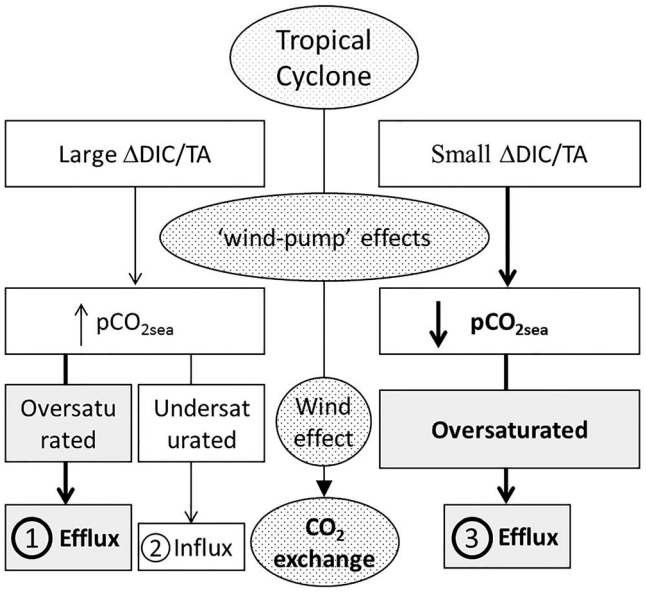

Figure 12. Conceptual diagram illustrating the mechanisms of TC-induced pCO_{2sea} change and CO_2 exchange. The thick arrows and bold words indicated significant responses to TC. TC = tropical cyclone; DIC = dissolved inorganic carbon; TA = total alkalinity.

CO_2 m^{-2} day^{-1}. The loss of CO_2 from the ocean (efflux) was about 19.08 ± 3.82 mmol CO_2/m^2 in 8 days. The results during Roanu differ from the previous study in the global ocean based on a state-of-the art global ocean biochemical model driven by 1,663 TCs (Levy et al., 2012). Levy et al. (2012) reported that in global ocean, TCs weakly affect the CO_2 efflux in supersaturated areas (high pCO_{2sea}). The BoB was hit by about three TCs during the postmonsoon and one TC during the premonsoon (Neetu et al., 2012). Extrapolating from the mean enhanced F_{CO2} of 3.91 ± 0.78 mmol CO_2/m^2 averaged from four TCs during the postmonsoon and of 19.08 ± 3.82 mmol CO_2/m^2 by one TC during the premonsoon, the total annual F_{CO2} induced by TCs was about 30.81 ± 6.16 mmol CO_2/m^2. The CO_2 efflux enhanced by TCs accounted for 55 ± 23% of the annual CO_2 efflux in the BoB, which is higher than the estimation of Levy et al. (2012) but very similar to the estimations in the Sargasso Sea (55%, Bates et al., 1998) and East China Sea (60%, Nemoto et al., 2009) during the summertime. Levy et al. (2012) estimated a contribution of 13.6% to the cyclonic season influx in the BoB. This may be because the effect of TC during the premonsoon was not considered in the estimation made by Levy et al. (2012).

The total TC-induced CO_2 efflux or influx is a function of the cyclone strength, size, structure, and oceanic and atmosphere conditions. High wind speeds accompanied by a TC enhance the gas transfer velocity and then increase the F_{CO2}. Previous studies demonstrated that the increase in the CO_2 efflux was mainly caused by the increase in wind speeds (Bates et al., 1998; Huang & Imberger, 2010; Nemoto et al., 2009) and the decrease in pCO_{2air} (Wada et al., 2013). The CO_2 efflux or influx induced by TCs depended on the CO_2 conditions at the time of the TC passage. In this study, the change of pCO_{2air} during all five TCs was within ±2.9 μatm, which was significantly lower than the value decreased (about 20 μatm) by typhoon Choi-wan (Wada et al., 2013). This could be because typhoon Choi-wan was about 40 km away to the mooring site, while the five TCs considered in this study were more than 183 km away from the mooring. Our results showed that the TC-generated CO_2 flux not only depended on the CO_2 conditions at the time of the TCs passage but also relied on the inorganic carbon conditions such as the ΔDIC/TA.

During the postmonsoon, the significantly enhanced CO_2 efflux from the ocean to the atmosphere in high pCO_{2sea} (oversaturated) conditions can be explained by the combination of two factors: (1) positive $dpCO_{2sea}$ after the TC passage due to large ΔDIC/TA (0.042–0.048) that supplies much DIC to the surface (wind effect); and (2) strong vertical mixing and upwelling (known as the wind-pump effects) generated by intense winds accompanied by a TC. The slightly changed F_{CO2} over undersaturated areas can be explained by the counteraction of the wind effect during TC and wind-pump effects after the TC. The significantly enhanced CO_2 efflux during the premonsoon in ultrahigh pCO_{2sea} (oversaturated) conditions was due to the wind effect, which greatly exceeded the role of wind-pump effects.

5. Conclusions

This study examined the storm-induced changes in both the partial pressure of CO_2 at the sea surface (pCO_{2sea}) and the air-sea CO_2 flux (F_{CO2}) during five TCs from November 2013 to January 2017 in the BoB. Analyses of meteorological, physical, and biological data showed three different mechanisms involved in the passage of the TC (Figure 12). The major conclusions from the present study include the following.

1. TCs with strong wind speeds (> 10 m/s) and shallow MLD (< 20 m) of the ocean before the storm tended to increase the pCO_{2sea} in the postmonsoon months (October–December) and to decrease the pCO_{2sea} in the premonsoon months (March–May).
2. The large value of ΔDIC/TA was the major cause for increases of the pCO_{2sea} induced by TCs in the postmonsoon months. The relatively small value of ΔDIC/TA was the major cause for the decreased pCO_{2sea} in the premonsoon months.

3. In the large ΔDIC/TA of the BoB waters, TCs with strong wind speeds significantly enhanced the CO_2 efflux in oversaturated areas, because of the combination of the wind effect during the storm and wind-pump effects after the storm (① in Figure 12). TCs slightly changed the F_{CO2} in undersaturated areas because of the counteraction of these two effects (② in Figure 12).

Over waters with small ΔDIC/TA, TCs significantly enhanced the CO_2 efflux in highly oversaturated conditions, because of the wind effect greatly exceeding the role of wind-pump effects (③ in Figure 12). In addition to the TC's intensity and CO_2 conditions when TC passage, the TC-generated F_{CO2} is affected by the inorganic carbon conditions such as the ΔDIC/TA.

4. Extrapolating from five TCs between November 2013 and January 2017, TCs in the BoB were estimated to contribute to a CO_2 efflux of 30.81±6.16 mmol CO_2/m^2. Our assumption is that TCs account for 55 ± 23% of the F_{CO2} over the BoB.

Acknowledgments
The authors are grateful to three anonymous reviewers for comments that helped significantly to improve this manuscript. This study was funded by the National Natural Sciences Foundation of China (41806146, 41876136, and 41430968) and the Collaborative Innovation Centre for 21st-Century Maritime Silk Road Studies (2015HS05). J. S. was supported by NSERC and OFI. Morozov Evgeny was supported by CAS President's International Fellowship Initiative (PIFI, 168422). Muhsan Ali Kalhoro was supported by China Postdoctoral fellowship programme (158563) and China Science and Technology Exchange Center, Ministry of Science and Technology for awarding Talented Young Scientist Award (PAK-16-021). Sufen Wang was supported by open fund of State Key Laboratory of Satellite Ocean Environment Dynamics, Second Institute of Oceanography (No. 0702). The authors thank the GTMBA Project Office of NOAA/PMEL for provision of the data (https://www.pmel.noaa.gov/) and appreciate Adrienne J. Sutton for her kind help with data processing and quality control. Argo floats data were collected and made freely available by the International Argo Program and the national programs that contribute to it (http://www.argo.ucsd.edu, http://argo.jcommops.org). The Argo Program is part of the Global Ocean Observing System.

References

Atlas, R., Hoffman, R. N., Ardizzone, J., Leidner, S. M., Jusem, J. C., Smith, D. K., & Gombos, D. (2011). A cross-calibrated, multiplatform ocean surface wind velocity product for meteorological and oceanographic applications. *Bulletin of the American Meteorological Society*, *92*(2), 157–174. https://doi.org/10.1175/2010BAMS2946.1

Bakker, D. C. E., Pfeil, B., Landa, C. S., Metzl, N., O'Brien, K. M., Olsen, A., et al. (2016). A multi-decade record of high-quality fCO_2 data in version 3 of the Surface Ocean CO_2 Atlas (SOCAT). *Earth System Science Data*, *8*(2), 383–413. https://doi.org/10.5194/essd-8-383-2016

Bates, N. R. (2007). Interannual variability of the oceanic CO_2 sink in the subtropical gyre of the North Atlantic Ocean over the last 2 decades. *Journal of Geophysical Research*, *112*, C09013. https://doi.org/10.1029/2006JC003759

Bates, N. R., Knap, A. H., & Michaels, A. F. (1998). Contribution of hurricanes to local and global estimates of air-sea exchange of CO_2. *Nature*, *395*(6697), 58–61. https://doi.org/10.1038/25703

Bates, N. R., Pequignet, A. C., & Sabine, C. L. (2006). Ocean carbon cycling in the Indian Ocean: 1. Spatio-temporal variability of inorganic carbon and air-sea CO_2 gas exchange. *Global Biogeochemical Cycles*, *20*, GB3020. https://doi.org/10.1029/2005GB002491

Bond, N. A., Cronin, M. F., Sabine, C., Kawai, Y., Ichikawa, H., Freitag, P., & Ronnholm, K. (2011). Upper Ocean response to typhoon Choi-wan as measured by the Kuroshio extension observatory mooring. *Journal of Geophysical Research*, *116*, C02031. https://doi.org/10.1029/2010JC006548

Chacko, N. (2017). Chlorophyll bloom in response to tropical cyclone Hudhud in the Bay of Bengal: Bio-Argo subsurface observations. *Deep Sea Research, Part I*, *124*, 66–72. https://doi.org/10.1016/j.dsr.2017.04.010

Chen, F. Z., Cai, W. J., Benitez-Nelson, C., & Wang, Y. C. (2007). Sea surface pCO_2-SST relationships across a cold-core cyclonic eddy: Implications for understanding regional variability and air-sea gas exchange. *Geophysical Research Letters*, *34*, L10603. https://doi.org/10.1029/2006GL028058

Chen, X., Pan, D., Bai, Y., He, X., Chen, C. A., & Hao, Z. (2013). Episodic phytoplankton bloom events in the Bay of Bengal triggered by multiple forcings. *Deep Sea Research, Part I*, *73*, 17–30. https://doi.org/10.1016/j.dsr.2012.11.011

Dickson, A. G., Sabine, C. L., & Christian, J. R. (Eds.) (2007). *Guide to best practices for ocean CO_2 measurements, PICES spec. Publ.* (Vol. 3, p. 191). Oak Ridge, TN: Carbon Dioxide Inf. Anal. Cent.

Fassbender, A. J., Sabine, C. L., Cronin, M. F., & Sutton, A. J. (2017). Mixed-layer carbon cycling at the Kuroshio extension observatory. *Global Biogeochemical Cycles*, *31*, 272–288. https://doi.org/10.1002/2016GB005547

Girishkumar, M. S., Suprit, K., Chiranjivi, J., Bhaskar, T. U., Ravichandran, M., Shesu, R. V., & Rao, E. P. R. (2014). Observed oceanic response to tropical cyclone Jal from a moored buoy in the south-western Bay of Bengal. *Ocean Dynamics*, *64*(3), 325–335. https://doi.org/10.1007/s10236-014-0689-6

Goyet, C., Coatanoan, C., Eischeid, G., Amaoka, T., Okuda, K., Healy, R., & Tsunogai, S. (1999). Spatial variation of total CO_2 and total alkalinity in the northern Indian Ocean: A novel approach for the quantification of anthropogenic CO_2 in seawater. *Journal of Marine Research*, *57*(1), 135–163. https://doi.org/10.1357/002224099765038599

Goyet, C., Millero, F. J., Poisson, A., & Shafer, D. K. (1993). Temperature dependence of CO_2 fugacity in seawater. *Marine Chemistry*, *44*(2-4), 205–219. https://doi.org/10.1016/0304-4203(93)90203-Z

Huang, P., & Imberger, J. (2010). Variation of pCO_2 in ocean surface water in response to the passage of a hurricane. *Journal of Geophysical Research*, *115*, C10024. https://doi.org/10.1029/2010JC006185

Keeling, C. D., Brix, H., & Gruber, N. (2004). Seasonal and long-term dynamics of the upper ocean carbon cycle at station ALOHA near Hawaii. *Global Biogeochemical Cycles*, *18*, GB4006. https://doi.org/10.1029/2004GB002227

Large, W. G., & Pond, S. (1981). Open ocean momentum flux measurements in moderate to strong winds. *Journal of Physical Oceanography*, *11*(3), 324–336. https://doi.org/10.1175/1520-0485(1981)011<0324:OOMFMI>2.0.CO;2

Le Quéré, C., Andrew, R. M., Canadell, J. G., Sitch, S., Korsbakken, J. I., Peters, G. P., et al. (2016). Global carbon budget 2016. *Earth System Science Data*, *8*, 605–649. https://doi.org/10.5194/essd-8-605-2016

Le Quéré, C., Raupach, M. R., Canadell, J. G., Marland, G., Bopp, L., Ciais, P., Conway, T. J., et al. (2009). Trends in the sources and sinks of carbon dioxide. *Nature Geoscience*, *2*(12), 831–836. https://doi.org/10.1038/ngeo689

Levitus, S. (1982). *Climatological atlas of the world ocean*, *NOAA Prof. Pap.* (Vol. 13, p. 173). Washington, DC: U.S. Govt. Printing Off.

Levy, M., Lengaigne, M., Bopp, L., Vincent, E. M., Madec, G., Éthé, C., Kumar, D., et al. (2012). Contribution of tropical cyclones to the air-sea CO_2 flux: A global view. *Global Biogeochemical Cycles*, *26*, GB2001. https://doi.org/10.1029/2011GB004145

Lonfat, M., Marks, F. D. Jr., & Chen, S. S. (2004). Precipitation distribution in tropical cyclones using the Tropical Rainfall Measuring Mission (TRMM) microwave imager: A global perspective. *Monthly Weather Review*, *132*(7), 1645–1660. https://doi.org/10.1175/1520-0493(2004)132<1645:PDITCU>2.0.CO;2

Maneesha, K., Murty, V. S. N., Ravichandran, M., Lee, T., Yu, W., & McPhaden, M. J. (2012). Upper ocean variability in the Bay of Bengal during the tropical cyclones Nargis and Laila. *Progress in Oceanography*, *106*, 49–61. https://doi.org/10.1016/j.pocean.2012.06.006

McPhaden, M. J., Meyers, G., Ando, K., Masumoto, Y., Murty, V. S. N., et al. (2009). RAMA: The research moored array for African–Asian–Australian monsoon analysis and prediction. *Bulletin of the American Meteorological Society*, *90*(4), 459–480. https://doi.org/10.1175/2008BAMS2608.1

Neetu, S., Lengaigne, M., Vincent, E. M., Vialard, J., Madec, G., Samson, G., et al. (2012). Influence of upper-ocean stratification on tropical cyclone-induced surface cooling in the Bay of Bengal. *Journal of Geophysical Research*, *117*, C12020. https://doi.org/10.1029/2012JC008433

Nemoto, K., Midorikawa, T., Wada, A., Ogawa, K., Takatani, S., Kimoto, H., et al. (2009). Continuous observations of atmospheric and oceanic CO_2 using a moored buoy in the East China Sea: Variations during the passage of typhoons. *Deep Sea Research, Part II*, *56*(8–10), 542–553. https://doi.org/10.1016/j.dsr2.2008.12.015

Obasi, G. O. P. (1997). WMO's programme on tropical cyclone. *Mausam*, *48*, 103–112.

Perrie, W., Zhang, W., Ren, X., Long, Z., & Hare, J. (2004). The role of midlatitude storms on air-sea exchange of CO_2. *Geophysical Research Letters*, *31*, L09306. https://doi.org/10.1029/2003GL019212

Rao, R. R., & Sivakumar, R. (2003). Seasonal variability of sea surface salinity and salt budget of the mixed layer of the North Indian Ocean. *Journal of Geophysical Research*, *108*(C1), 3009. https://doi.org/10.1029/2001JC000907

Sabine, C. L., Key, R. M., Feely, R. A., & Greeley, D. (2002). Inorganic carbon in the Indian Ocean: Distribution and dissolution processes. *Global Biogeochemical Cycles*, *16*(4), 1067. https://doi.org/10.1029/2002GB001869

Sarangi, R. K., Mishra, M. K., & Chauhan, P. (2015). Remote sensing observations on imapct of Phailin cyclone on phytoplankton distribution in northern Bay of Bengal. *IEEE*, *8*(2), 539–549. https://doi.org/10.1109/JSTARS.2014.2347036

Sarma, V. V. S. S., Lenton, A., Law, R. M., Metzl, N., Patra, P. K., Doney, S., et al. (2013). Sea–air CO_2 fluxes in the Indian Ocean between 1990 and 2009. *Biogeosciences*, *10*(11), 7035–7052. https://doi.org/10.5194/bg-10-7035-2013

Sarmiento, J. L., & Gruber, N. (2006). *Ocean biogeochemical dynamics* (p. 526). Princeton, NJ: Princeton University Press.

Sengupta, D., Bharathraj, G. N., & Shenoi, S. S. C. (2006). Surface freshwater from Bay of Bengal runoff and Indonesian throughflow in the tropical Indian Ocean. *Geophysical Research Letters*, *33*, L22609. https://doi.org/10.1029/2006GL027573

Sengupta, D., Goddalehundi, B. R., & Anitha, D. (2008). Cyclone-induced mixing does not cool SST in the post-monsoon north Bay of Bengal. *Atmospheric Science Letters*, *9*(1), 1–6. https://doi.org/10.1002/asl.162

Sheng, J., Zhai, X., & Greatbatch, R. J. (2006). Numerical study of the storm-induced circulation on the Scotian shelf during Hurricane Juan using a nested-grid ocean model. *Progress in Oceanography*, *70*(2-4), 233–254. https://doi.org/10.1016/j.pocean.2005.07.007

Song, Y. J., & Tang, D. L. (2017). Mixed layer depth responses to tropical cyclones Kalmaegi and Fung-Wong in the northeastern South China Sea. *Journal of Tropical Oceanography*, *36*(1), 15–24. https://doi.org/10.11978/2016045

Sun, Q. Y., Tang, D. L., Legendre, L., & Shi, P. (2014). Enhanced sea-air CO_2 exchange influenced by a tropical depression in the South China Sea. *Journal of Geophysical Research: Oceans*, *119*, 6792–6804. https://doi.org/10.1002/2014JC010131

Sutton, A. J., Sabine, C. L., Dietrich, C., Maenner, S., Musielewicz, S., Bott, R., & Osborne, J. (2017). Partial pressure (or fugacity) of carbon dioxide, pH (on total scale), salinity and other variables collected from time series observations using Bubble type equilibrator for autonomous carbon dioxide (CO_2) measurement, Carbon dioxide (CO_2) gas analyzer and other instruments from MOORING BOBOA_90E_15N deployments 1, 2 and 3 in the Bay of Bengal, Indian Ocean from 2013-11-24 to 2017-01-09 (NCEI Accession 0162473). Version 2.2. NOAA National Centers for Environmental Information. Dataset. https://doi.org/10.7289/V5H70D1K

Sutton, A. J., Sabine, C. L., Feely, R. A., Cai, W. J., Cronin, M. F., McPhaden, M. J., et al. (2016). Using present-day observations to detect when anthropogenic change forces surface ocean carbonate chemistry outside preindustrial bounds. *Biogeosciences*, *13*(17), 5065–5083. https://doi.org/10.5194/bg-13-5065-2016

Sutton, A. J., Sabine, C. L., Maenner, S., Lawrence, N., Meinig, C., Feely, R. A., et al. (2014). A high-frequency atmospheric and seawater pCO_2 data set from 14 open-ocean sites using a moored autonomous system. *Earth System Science Data*, *6*(2), 353–366. https://doi.org/10.5194/essd-6-353-2014

Sutton, A. J., Wanninkhof, R., Sabine, C. L., Feely, R. A., Cronin, M. F., & Weller, R. A. (2017). Variability and trends in surface seawater pCO_2 and CO_2 flux in the Pacific Ocean. *Geophysical Research Letters*, *44*, 5627–5636. https://doi.org/10.1002/2017GL073814

Takahashi, T., Olafsson, J., Goddard, J. G., Chipman, D. W., & Sutherland, S. C. (1993). Seasonal-variation of CO_2 and nutrients in the high latitude surface oceans—A comparative-study. *Global Biogeochemical Cycles*, *7*(4), 843–878. https://doi.org/10.1029/93GB02263

Takahashi, T., Sutherland, S. C., Sweeney, C., Poisson, A., Metzl, N., Tilbrook, B., et al. (2002). Global sea-air CO_2 flux based on climatological surface ocean pCO_2, and seasonal biological and temperature effects. *Deep Sea Research, Part II*, *49*(9–10), 1601–1622. https://doi.org/10.1016/S0967-0645(02)00003-6

Takahashi, T., Sutherland, S. C., Wanninkhof, R., Sweeney, C., Feely, R. A., Chipman, D. W., et al. (2009). Climatological mean and decadal change in surface ocean pCO_2, and net sea-air CO_2 flux over the global oceans. *Deep Sea Research, Part II*, *56*(8-10), 554–577. https://doi.org/10.1016/j.dsr2.2008.12.009

Thadathil, P., Muraleedharan, P. M., Rao, R. R., Somayajulu, Y. K., Reddy, G. V., & Revichandran, C. (2007). Observed seasonal variability of barrier layer in the Bay of Bengal. *Journal of Geophysical Research*, *112*, C02009. https://doi.org/10.1029/2006JC003651

Turi, G., Lachkar, Z., & Gruber, N. (2014). Spatiotemporal variability and drivers of pCO2 and air-sea CO_2 fluxes in the California Current system: An eddy-resolving modeling study. *Biogeosciences*, *11*(3), 671–690. https://doi.org/10.5194/bg-11-671-2014

Vidya, P. J., & Das, S. (2017). Contrasting Chl-a responses to the tropical cyclones Thane and Phailin in the Bay of Bengal. *Journal of Marine Systems*, *165*, 103–114.

Wada, A., Cronin, M. F., Sutton, A. J., Kawai, Y., & Ishii, M. (2013). Numerical simulations of oceanic pCO_2 variations and interactions between Typhoon Choi-wan (0914) and the ocean. *Journal of Geophysical Research: Oceans*, *118*, 2667–2684. https://doi.org/10.1002/jgrc.20203

Wada, A., Midorikawa, T., Ishii, M., & Motoi, T. (2011). Carbon system changes in the East China Sea induced by Typhoons Tina and Winnie in 1997. *Journal of Geophysical Research*, *116*, C07014. https://doi.org/10.1029/2010JC006701

Wanninkhof, R. (1992). Relationship between wind speed and gas exchange over the ocean. *Journal of Geophysical Research*, *97*(C5), 7373–7382. https://doi.org/10.1029/92JC00188

Wanninkhof, R. (2014). Relationship between wind speed and gas exchange over the ocean revisited. *Limnology and Oceanography*, *12*(6), 351–362. https://doi.org/10.4319/lom.2014.12.351

Wanninkhof, R., Asher, W. E., Ho, D. T., Sweeney, C., & McGillis, W. R. (2009). Advances in quantifying air-sea gas exchange and environmental forcing. *Annual Review of Marine Science*, *1*(1), 213–244. https://doi.org/10.1146/annurev.marine.010908.163742

Wanninkhof, R., & McGillis, W. R. (1999). A cubic relationship between air-sea CO_2 exchange and wind speed. *Geophysical Research Letters*, *26*(13), 1889–1892. https://doi.org/10.1029/1999GL900363

Warner, S. J., Becherer, J., Pujiana, K., Shroyer, E. L., Ravichandran, M., Thangaprakash, V., & Moum, J. N. (2016). Monsoon mixing cycles in the Bay of Bengal: A year-long subsurface mixing record. *Oceanography*, *29*(2), 158–169. https://doi.org/10.5670/oceanog.2016.48

Weiss, R. F. (1974). Carbon dioxide in water and seawater: The solubility of a non-ideal gas. *Marine Chemistry*, *2*(3), 203–215. https://doi.org/10.1016/0304-4203(74)90015-2

Ye, H. J., Kalhoro, M. A., Morozov, E., Tang, D. L., Wang, S. F., & Thies, P. R. (2017). Increased chlorophyll-a concentration in the South China Sea caused by occasional sea surface temperature fronts at peripheries of eddies. *International Journal of Remote Sensing*, *39*(13), 4360–4375. https://doi.org/10.1080/01431161.2017.1399479

Ye, H. J., Sheng, J., Tang, D. L., Eko, S., Kalhoro, M. A., & Sui, Y. (2017). Storm-induced changes in pCO_2 at the sea surface over the northern South China Sea during Typhoon Wutip. *Journal of Geophysical Research: Oceans*, *122*, 4761–4778. https://doi.org/10.1002/2016JC012643

Ye, H. J., Sui, Y., Tang, D. L., & Afanasyev, Y. (2013). A subsurface chlorophyll *a* bloom induced by typhoon in the South China Sea. *Journal of Marine Systems*, *128*, 138–145. https://doi.org/10.1016/j.jmarsys.2013.04.010